



**FACULTY  
OF MATHEMATICS  
AND PHYSICS**  
Charles University

**MASTER THESIS**

Martin Sýkora

**Hamiltonian and thermodynamic theory  
of solids and fluids**

Mathematical Institute of Charles University

Supervisor of the master thesis: RNDr. Michal Pavelka, Ph.D.

Study programme: Mathematics

Study branch: Mathematical Modelling in Physics and  
Technology

Prague 2019

I declare that I carried out this master thesis independently, and only with the cited sources, literature and other professional sources.

I understand that my work relates to the rights and obligations under the Act No. 121/2000 Sb., the Copyright Act, as amended, in particular the fact that the Charles University has the right to conclude a license agreement on the use of this work as a school work pursuant to Section 60 subsection 1 of the Copyright Act.

Prague, 19<sup>th</sup> July, 2019

Martin Sýkora

I would like to express my thanks to all those, who have helped me finish this thesis. At first, I have to mention my supervisor, Dr. Michal Pavelka, who taught me nearly everything I know about GENERIC. I heartily thank him for his support and willingness to help even during his free time. I am also grateful to Dr. Jaroslav Hron and Dr. Sebastian Schwarzacher for their consultations.

Next, I would like to thank my friends, especially Petr Pelech, whose interest in the topic and ideas about it have helped me multiple times, and many fellow organizers of the PraSe seminar for proof-reading and both moral and factual support.

Last but not least, I thank my parents for their parental support and my brother for his patient replies to my abundant needles questions.

This work was supported by Czech Science Foundation, Project No. 17-15498Y.

Title: Hamiltonian and thermodynamic theory of solids and fluids

Author: Martin Sýkora

Institute: Mathematical Institute of Charles University

Supervisor: RNDr. Michal Pavelka, Ph.D., Mathematical Institute of Charles University

Abstract: The standard approach to modelling mechanics of continuum based on balances of mass, momentum, angular momentum and energy is a very powerful tool. However, there is no connection between that and the Hamiltonian mechanics, that superbly describes kinematics of isolated particles. Thus, the two topics are rather isolated. Nevertheless, there is another approach to continuum mechanics – a one, whose reversible part is based on Hamiltonian mechanics, while the irreversible is generated by a dissipation potential.

This framework, called GENERIC, is thus an interesting bridge between continuous and discrete systems. In this thesis, we present the GENERIC framework applied to a continuous body, derive the governing equations and compare them to the standard theory. Both analytical and numerical solutions to a decent range of model examples are presented and analysed.

Keywords: Non-equilibrium thermodynamics, GENERIC, Eulerian description, Hamiltonian, Dissipation potential

# Contents

<b>Introduction</b>	<b>2</b>
<b>Nomenclature</b>	<b>4</b>
<b>1 Hamiltonian Mechanics</b>	<b>6</b>
1.1 Hamiltonian Mechanics of a Single Particle . . . . .	6
1.2 Hamiltonian Mechanics of Continuum . . . . .	7
1.3 From Lagrange to Euler . . . . .	8
1.4 Equations Involving the Left Cauchy-Green Tensor . . . . .	9
1.5 Comparison to neo-Hookean Solids . . . . .	12
1.6 Equations Involving the Distortion Matrix . . . . .	13
1.7 Properties of the Pressure . . . . .	15
<b>2 Thermodynamics</b>	<b>17</b>
2.1 Addition of Dissipation . . . . .	17
2.2 Fundamental Relation . . . . .	18
2.3 Dissipation Potential . . . . .	18
2.4 Final Form of the Governing Equations . . . . .	20
<b>3 Examples</b>	<b>23</b>
3.1 Neo-Hookean Solid in One Dimension . . . . .	23
3.2 Vertical Vibrations under the neo-Hookean Model . . . . .	25
3.3 Vertical Vibrations under the SHTC Model . . . . .	26
3.4 Numerical Solution to the Vibrations under SHTC Model . . . . .	28
3.5 Elastoplastic Vibrations . . . . .	29
3.6 Simple Shear . . . . .	35
3.7 Elastoplastic Solid in Two Dimensions . . . . .	41
3.8 Couette Flow . . . . .	41
<b>Conclusion</b>	<b>46</b>
<b>Bibliography</b>	<b>47</b>
<b>List of Figures</b>	<b>49</b>
<b>List of Tables</b>	<b>52</b>
<b>A Attachments</b>	<b>53</b>
A.1 Functional Derivative . . . . .	53
A.2 Derivation of the Governing Equations . . . . .	54
A.3 Model with Distortion Describes the neo-Hookean Solids . . . . .	55
A.4 Numerical Scheme . . . . .	56
A.5 Material Properties . . . . .	59

# Introduction

## Background

The reader is assumed to have at least a basic knowledge of continuum mechanics, especially the concepts of reference and actual<sup>1</sup> configuration and Lagrangian and Eulerian description.<sup>2</sup> Those, who do not, are recommended to study about the topic in literature. A nice book is written by Gurtin et al. [2010]. Here, we only present an extremely brief summary:

We model a continuous body, which occupies at time  $t$  a domain  $\Omega(t)$ . This is called the actual configuration. We also assume to have a reference configuration  $\Omega_0$  such that position of each particle at each time is given by a function  $\mathbf{x} = \mathbf{x}(\mathbf{X}, t)$ ,  $\mathbf{X} \in \Omega_0$ , that is,  $\mathbf{x}(\Omega_0, t) = \Omega(t)$ . Everything ( $\Omega(t)$ ,  $\Omega_0$  and the mapping between them) is assumed to be “nice” – domains have smooth boundaries, mappings are smooth, bijective and so on. Thus, we also have the inverse mapping  $\mathbf{X}(\mathbf{x}, t)$ . We often omit  $t$  for brevity and set  $\Omega_0 = \Omega(0)$ .

Since a real material is modelled, the body is equipped with some fields describing it – for instance the mass density  $\rho$ . Anything written in terms of the reference configuration is called Lagrangian, while anything written in terms of the actual configuration is called Eulerian. Thus,  $\rho(\mathbf{x}, t)$  is an Eulerian function and  $\rho(\mathbf{X}, t) (= \rho(\mathbf{x}(\mathbf{X}, t), t))$  is a Lagrangian function.

In the usual framework, balance equations are usually formulated in an integral form<sup>3</sup>, which give after some computations the Eulerian balance equations:

$$\begin{aligned}\frac{\partial \rho}{\partial t} + \operatorname{div}(\rho \mathbf{v}) &= 0, \\ \frac{\partial \mathbf{m}}{\partial t} + \operatorname{div}(\mathbf{m} \otimes \mathbf{v}) &= \operatorname{div}(\mathbb{T}) + \rho \mathbf{f}.\end{aligned}$$

Here,  $\mathbf{v}$  is the (Eulerian) velocity field and  $\mathbf{m} = \rho \mathbf{v}$  is the momentum density. The Cauchy stress tensor  $\mathbb{T}$  describes the inner forces within the body (e.g. resulting from the deformation of the body), while  $\mathbf{f}$  is the density of outer forces, such as gravity. Balance of energy is also stated as

$$\frac{\partial \varepsilon}{\partial t} + \operatorname{div}(\varepsilon \mathbf{v}) = \operatorname{div}(\mathbb{T} \mathbf{v}) + \rho \mathbf{f} \cdot \mathbf{v} + \rho q - \operatorname{div}(\mathbf{j}_e),$$

where  $q$  are the heat sources and  $\mathbf{j}_e$  the heat fluxes. We neglect them in the following chapters.

Finally, the Cauchy stress tensor (i.e. the material of the body) must be specified to close the system. This is called the constitutive relation. The so called compressible elastic neo-Hookean model sets for example  $\mathbb{T} = \rho \mu (\mathbb{B} - \mathbb{I})$ ,  $\mathbb{B} = \mathbb{F} \mathbb{F}^\top$ ,  $\mathbb{F} = \frac{\partial \mathbf{x}}{\partial \mathbf{X}}$ . For the derivation of this relation, see section 1.5. However, many more constitutive relations are often derived from variety of physical ansatzes, principles of frame and material frame indifference or thermodynamic approaches.

---

<sup>1</sup>Also known as current configuration.

<sup>2</sup>Other topics that may be necessary to fully understand this text are the basics of thermodynamics and Hamiltonian mechanics.

<sup>3</sup>For example, the balance of mass stating that the mass of the body does not change reads  $\frac{d}{dt} \int_{\Omega(t)} \rho(\mathbf{x}, t) d\mathbf{x} = 0$ .

# Objectives and Motivations

Usually, mechanics of continuum is modelled in the way described in the previous section, often expressing the Cauchy stress tensor in terms of the left Cauchy-Green tensor  $\mathbb{B}$  or the symmetric velocity gradient  $\mathbb{D}$ . Examples of such models include the already mentioned neo-Hookean solid, as well as Maxwell and Oldroyd-B solids, that are commented for instance by Málek et al. [2015]. Fluids are often described by Navier-Stokes model or its generalizations. Polymeric fluids are well described by Bird et al. [1987]. This concept is successful from many points of view, however, it is, in a way, isolated from the mechanics of isolated particles, which is surprisingly elegantly described by Hamiltonian mechanics. A derivation of the governing equations that would generalize the isolated-particles-case would be a very interesting alternative from a physical point of view.

Indeed, there is such framework, which we shall study in this text. To be more specific, we follow the GENERIC<sup>4</sup> framework, i.e., divide the evolution into reversible and irreversible part. The reversible part is derived from Hamiltonian mechanics and Poisson brackets, see chapter 1, while the irreversible is generated by a functional called the dissipation potential in chapter 2. As for the reversible part, we derive three sets of governing equations, involving  $\mathbb{F}$ ,  $\mathbb{B}$  and the distortion matrix  $\mathbb{A} = \mathbb{F}^{-1}$ ,<sup>5</sup> respectively. All of them are in the Eulerian frame as the neo-Hookean model. We briefly work with the equations involving  $\mathbb{B}$  to demonstrate that they can describe an elastic neo-Hookean solid.

We then focus on the equations with distortion  $\mathbb{A}$ , add the irreversible part and thus formulate the so-called SHTC<sup>6</sup> model – and examine it. This model is well described by Dumbser et al. [2016] and Dumbser et al. [2017]. An interesting physical motivation of the model is presented by Peshkov et al. [2017]. An advantage of this framework is that in the case of reversible evolution, the distortion matrix represents the connection between reference and actual configurations and tracking of the particles is thus not necessary. As we will demonstrate, this property is, however, lost once the dissipation is added. A potential interpretation of  $\mathbb{A}$  in a system with dissipation is discussed in section 3.6. Another possible advantage of the distortion matrix  $A$  is the fact, that it has nine degrees of freedom. Thus, this description is rich and capable of dealing with anisotropy of material without adding new variables. We, however, do not study anisotropy. This problem is addressed for instance by Peshkov et al. [2019] or Sedov [1965].

The SHTC model describes both solids and fluids, which we demonstrate. Both analytic and numerical solutions of a few model examples are presented. Purely one-dimensional motion is studied and compared to neo-Hookean solids. Numerical solutions are then compared to one-dimensional wave equation. Next, the relation of shear rate and shear stress is computed in a simple shear in both elastic and elastoplastic solid. A planar motion in an elastoplastic solid is then briefly studied to demonstrate that  $\text{curl}(\mathbb{A})$  does not have to be equal to zero if the dissipation is added. Finally, Couette flow is numerically simulated to show the ability of the SHTC model to describe fluids.

---

<sup>4</sup>Stands for “General Equation for Non-Equilibrium Reversible-Irreversible Coupling”. It was first introduced by Grmela and Öttinger [1997] and Öttinger and Grmela [1997].

<sup>5</sup>This definition is used to derive the equations without dissipation. It is violated by the dissipation and  $\mathbb{A}$  becomes just a matrix variable in the equations. See section 2.1.

<sup>6</sup>Stands for “Symmetric Hyperbolic Thermodynamically Compatible”.

# Nomenclature

## Important Symbols

Symbol	Equivalent	Name
$\mathbf{x}$	$(x, y, z)^\top$	Current position vector
$\mathbf{X}$	$(X, Y, Z)^\top$	Reference position vector
$t$	...	Time
$\rho$	...	Mass density
$\rho_0$	...	Reference density
$\mathbf{v}$	...	Velocity
$\mathbf{m}$	$\rho\mathbf{v}$	Linear momentum density per volume
$\mathbb{F}$	$\frac{\partial \mathbf{x}}{\partial \mathbf{X}}$	Deformation gradient
$\mathbb{A}$	$\mathbb{F}^{-1}$	Distortion matrix
$\mathbb{B}$	$\mathbb{F}\mathbb{F}^\top$	Left Cauchy-Green tensor
$\mathbb{G}$	$\mathbb{A}^\top\mathbb{A}$	...
$\mathbb{L}$	$\nabla\mathbf{v}$	Velocity gradient
$\mathbb{D}$	$0.5(\mathbb{L} + \mathbb{L}^\top)$	Symmetric velocity gradient
$\varepsilon$	...	Total energy density per volume
$e$	$\frac{\varepsilon}{\rho}$	Total energy density per mass
$e_{\text{kin}}$	...	Kinetic energy per mass
$e_{\text{meso}}$	...	Mesoscale, or elastic, energy per mass
$e_{\text{micro}}$	...	Microscale energy; equation of state per mass
$e_1$	$e_{\text{micro}} + e_{\text{meso}}$	Internal energy per mass
$E$	$\int \varepsilon d\mathbf{x}$	Total energy
$s$	...	Entropy density per volume
$\varsigma$	$\frac{s}{\rho}$	Entropy density per mass
$p$	$\rho^2 \left( \frac{\partial e_{\text{micro}}}{\partial \rho} \right)_\varsigma$	Pressure
$p_0$	...	Reference pressure
$\sigma$	$-\mathbb{A}^\top E_{\mathbb{A}}$	...
$\mathbb{T}$	$-p\mathbb{I} + \sigma$	Cauchy stress tensor
$T$	$\frac{\partial e_1}{\partial \varsigma}$	Temperature
$c_p$	...	Specific heat capacity at constant pressure
$c_v$	...	Specific heat capacity at constant volume
$c_s$	...	Characteristic velocity of transverse perturbations
$c_0$	...	Adiabatic speed of sound
$\gamma$	$\frac{c_p}{c_v}$	Ratio of specific heat capacities
$\delta$	...	Kronecker delta
$\frac{\delta F}{\delta f}$	...	Functional derivative of $F$ with respect to $f$ ; see appendix A.1
$T^{\text{ref}}$	...	Reference temperature in the Mie-Gruneisen energy
$\Gamma_0$	...	A constant in the Shock Mie-Gruneisen energy
$u$	...	A constant in the Shock Mie-Gruneisen energy
$\tau_0$	...	A constant in dissipation term for solids
$\sigma_0$	...	A constant in dissipation term for solids
$n$	...	A constant in dissipation term for solids
$\mu$	...	Dynamic viscosity

## Abbreviations

GENERIC	General Equation for Non-Equilibrium Reversible-Irreversible Coupling
SHTC	Symmetric Hyperbolic Thermodynamically Compatible
ADER	Advection-Diffusion-Reaction
WENO	Weighted Essentially Non-Oscillatory
EOS	Equation of State
BC	Boundary Conditions
IC	Initial Conditions
WLOG	Without Loss of Generality

## Collisions of Notation

The author is aware of one collision in notation:  $\mu$  has the meaning of both dynamic viscosity and a parameter in a the neo-Hookean model. The reason for that is that this agrees with standard notation. Moreover, the two are never mixed together. The neo-Hookean solid is only mentioned in the elastic models in chapter 1, section 3.1 and appendix A.3. On the other hand, viscosity is connected only with dissipation for fluids and is mentioned in chapter 2, section 3.8 and appendix A.5.

## Other Conventions

Tensorial and differential operators such as transpose or inverse matrix, matrix product, divergence, gradient etc. follow their standard definitions. Divergence of a matrix is assumed row-wise, that is  $\text{div}(\mathbb{M}) = (\text{div}(\mathbf{M}_1), \text{div}(\mathbf{M}_2), \text{div}(\mathbf{M}_3))^\top$  for any matrix  $\mathbb{M}$  with rows  $\mathbf{M}_1$ ,  $\mathbf{M}_2$  and  $\mathbf{M}_3$ . The determinant is denoted by  $\det$  or sometimes by  $|\bullet|$  for brevity. The symbol  $\|\bullet\|_F$  stands for Frobenius norm.

Unless stated otherwise, Einstein summation convention is applied, that is, repeated indexes are to be summed over.

# 1. Hamiltonian Mechanics

## 1.1 Hamiltonian Mechanics of a Single Particle

In this section, we will briefly summarize one of the many methods to describe the mechanics of a single particle. Note that in the following section we use a very similar method to describe the mechanics of continuum.

Having a particle in space, let us denote  $\mathbf{q}$  its generalized position and  $\mathbf{p}$  its generalized momentum.<sup>1</sup> Let us further denote  $H(\mathbf{q}, \mathbf{p})$  the so called Hamiltonian, i.e., the mechanical energy of the particle expressed in the terms of generalized positions and momenta. Then the time evolution of  $\mathbf{q}$  and  $\mathbf{p}$  is given by Hamilton's equations

$$\begin{pmatrix} \dot{\mathbf{q}} \\ \dot{\mathbf{p}} \end{pmatrix} = \begin{pmatrix} 0 & \mathbb{I} \\ -\mathbb{I} & 0 \end{pmatrix} \cdot \begin{pmatrix} H_{\mathbf{q}} \\ H_{\mathbf{p}} \end{pmatrix},$$

where subscripts stand for partial derivatives. These equations are equivalent to Newton's second law of motion.

As an example, we describe the motion of a particle falling in the homogeneous gravitational field. That is,  $q$  is the point's altitude,  $p$  its vertical momentum and the energy is expressed as  $H(q, p) = gmq + \frac{1}{2m}p^2$ , where  $m$  denotes the point's mass. The time evolution for  $q$  and  $p$  then read as

$$\dot{q} = \frac{1}{m}p,$$

$$\dot{p} = -gm.$$

Now let us consider an arbitrary functional  $A(\mathbf{q}, \mathbf{p})$  describing some property of the particle, for example its kinetic energy. Then its time evolution may be expressed by the chain rule as

$$\dot{A} = (A_{\mathbf{q}}, A_{\mathbf{p}}) \cdot \begin{pmatrix} \dot{\mathbf{q}} \\ \dot{\mathbf{p}} \end{pmatrix} = (A_{\mathbf{q}}, A_{\mathbf{p}}) \cdot \begin{pmatrix} 0 & \mathbb{I} \\ -\mathbb{I} & 0 \end{pmatrix} \begin{pmatrix} H_{\mathbf{q}} \\ H_{\mathbf{p}} \end{pmatrix} = \{A, H\}^{(C)},$$

where  $\{A, H\}^{(C)}$  is the canonical Poisson bracket defined for any two functionals  $A(\mathbf{q}, \mathbf{p})$  and  $B(\mathbf{q}, \mathbf{p})$  as

$$\{A, B\}^{(C)} \stackrel{\text{def}}{=} \frac{\partial A}{\partial \mathbf{q}} \cdot \frac{\partial B}{\partial \mathbf{p}} - \frac{\partial A}{\partial \mathbf{p}} \cdot \frac{\partial B}{\partial \mathbf{q}}.$$

To summarize, Hamilton's equations (or Newton's second law) imply that the time evolution of any functional  $A$  is described by the canonical Poisson bracket of  $A$  and the Hamiltonian  $H$ .

However, this implication may be reversed. We postulate that the canonical Poisson bracket defines the time evolution of an arbitrary functional  $A(\mathbf{q}, \mathbf{p})$  and proceed as follows:

---

<sup>1</sup>Generalized positions and momenta are  $N$ -dimensional vector spaces uniquely describing the position and momentum of the particle respectively in any coordinate systems.

Calculating the time derivative of  $A$  by both the Poisson bracket and the chain rule, we get

$$\begin{aligned}\dot{A} &= \{A, H\}^{(C)} = \frac{\partial A}{\partial \mathbf{q}} \cdot \frac{\partial H}{\partial \mathbf{p}} + \frac{\partial A}{\partial \mathbf{p}} \cdot \frac{\partial H}{\partial \mathbf{q}}, \\ \dot{A} &= \frac{\partial A}{\partial \mathbf{q}} \cdot \dot{\mathbf{q}} - \frac{\partial A}{\partial \mathbf{p}} \cdot \dot{\mathbf{p}}.\end{aligned}$$

Comparing these two and using the fact, that  $A$  may be arbitrary (namely  $A(\mathbf{q}, \mathbf{p}) = q_i$  and  $A(\mathbf{q}, \mathbf{p}) = p_i$  for  $i = 1, 2, \dots, N$ ), we get

$$\begin{aligned}\dot{\mathbf{q}} &= \frac{\partial H}{\partial \mathbf{p}}, \\ \dot{\mathbf{p}} &= -\frac{\partial H}{\partial \mathbf{q}},\end{aligned}$$

which are the Hamilton's equations.

This widely known result may be summarized this way: If we prescribe the canonical Poisson bracket of two functionals depending on generalized positions and momenta and postulate that the Poisson bracket describes the time evolution in the sense specified above, we get the equations describing the time evolutions of the generalized positions and momenta.<sup>2</sup> In the next section of this work, we will try to mimic this procedure for continuum instead of a single particle.

## 1.2 Hamiltonian Mechanics of Continuum

To follow the idea of the previous section, in order to obtain the evolution equations for continuum, we need to know what Poisson bracket describes the time evolution. To find it, we may first focus on finitely many particles.

Let us have  $n$  particles with (generalized) positions and momenta  $\mathbf{q}_\alpha$  and  $\mathbf{p}_\alpha$  for  $\alpha = 1, 2, \dots, n$ . Then the canonical Poisson bracket can be generalized to

$$\{A, B\}^{(C)} \stackrel{\text{def}}{=} \sum_{\alpha=1}^n \frac{\partial A}{\partial \mathbf{q}_\alpha} \cdot \frac{\partial B}{\partial \mathbf{p}_\alpha} - \frac{\partial A}{\partial \mathbf{p}_\alpha} \cdot \frac{\partial B}{\partial \mathbf{q}_\alpha}.$$

The concept of continuum may be viewed as describing a body by a system of infinitely many particles which have their position, speed and mass density instead of mass. If we do so, the index of an isolated particle is naturally replaced by Lagrangian position of the material point  $\mathbf{X}$ , the position of the particles has analogy in the Eulerian position of the material point  $\mathbf{x}(\mathbf{X}, t)$  and the momentum of a particle transform to the momentum density per Lagrangian volume  $\mathbf{M}(\mathbf{X}, t)$ .<sup>3</sup> Furthermore, the sum over  $\alpha$  becomes an integral over Lagrangian volume, and partial derivatives become functional derivatives<sup>4</sup>. We may then introduce a Poisson bracket in the Lagrangian frame, depending on functionals  $A(\mathbf{x}, \mathbf{M})$  and  $B(\mathbf{x}, \mathbf{M})$ , as

---

<sup>2</sup>These equations are written in terms of the Hamiltonian  $H$ , so one also need to know its form to close the system.

<sup>3</sup>From now on, we will for brevity omit the explicit time-dependency of any function from our notation.

<sup>4</sup>See appendix A.1 for its definition.

$$\{A, B\}^{(L)} \stackrel{\text{def}}{=} \int \frac{\delta A}{\delta \mathbf{x}} \cdot \frac{\delta B}{\delta \mathbf{M}} - \frac{\delta A}{\delta \mathbf{M}} \cdot \frac{\delta B}{\delta \mathbf{x}} d\mathbf{X}.$$

This derivation of the Poisson bracket is definitely not rigorous and should be viewed as a motivation only. A more proper geometric justification is briefly presented by Pavelka et al. [2019].

### 1.3 From Lagrange to Euler

Having a Poisson bracket, one could get the time evolution for  $\mathbf{x}(\mathbf{X})$  and  $\mathbf{M}(\mathbf{X})$ , i.e., the evolution equations in Lagrangian frame. We would, however, like to get the equations in the Eulerian frame. To do so, we must first specify what state variables will we work with. We choose the fields

$$\begin{aligned} \rho(\mathbf{x}) &= \rho_0(\mathbf{X}(\mathbf{x})) \cdot \left| \frac{\partial \mathbf{X}}{\partial \mathbf{x}} \right|, \\ \mathbf{m}(\mathbf{x}) &= \mathbf{M}(\mathbf{X}(\mathbf{x})) \cdot \left| \frac{\partial \mathbf{X}}{\partial \mathbf{x}} \right|, \\ s(\mathbf{x}) &= s_0(\mathbf{X}(\mathbf{x})) \cdot \left| \frac{\partial \mathbf{X}}{\partial \mathbf{x}} \right|, \\ \mathbb{F}_{iI}(\mathbf{x}) &= \frac{\partial x_i}{\partial X_I} \Big|_{\mathbf{X}(\mathbf{x})} \end{aligned}$$

of Eulerian mass density, momentum density and entropy density per Eulerian volume and the deformation tensor. Here,  $\rho_0$  and  $s_0$  stand for volume densities of mass and entropy in the reference configuration and  $|\bullet|$  for the determinant.

By letting the functionals  $A$  and  $B$  depend on  $\rho$ ,  $\mathbf{m}$ ,  $s$  and  $\mathbb{F}$ , one may project<sup>5</sup> the Lagrangian Poisson bracket to an Eulerian one defined<sup>6</sup> as

$$\begin{aligned} \{A, B\}^{(E)} \stackrel{\text{def}}{=} \{A, B\}^{(\text{FM})} &+ \int F_{jI} (A_{F_{iI}} \partial_j B_{m_i} - B_{F_{iI}} \partial_j A_{m_i}) d\mathbf{x} \\ &- \int \partial_k F_{iI} (A_{F_{iI}} B_{m_k} - B_{F_{iI}} A_{m_k}) d\mathbf{x}, \end{aligned}$$

where the superscript (FM) stands for fluid mechanics defined as

$$\begin{aligned} \{A, B\}^{(\text{FM})} \stackrel{\text{def}}{=} \int \rho (\partial_i A_\rho B_{m_i} - \partial_i B_\rho A_{m_i}) d\mathbf{x} &+ \int m_i (\partial_j A_{m_i} B_{m_j} - \partial_j B_{m_i} A_{m_j}) d\mathbf{x} \\ &+ \int s (\partial_i A_s B_{m_i} - \partial_i B_s A_{m_i}) d\mathbf{x}. \end{aligned}$$

Here, the symbol  $\partial_i$  stands for partial derivative with respect to  $x_i$ , while the subscripts of  $A$  and  $B$  stand for functional derivatives.

Having the Poisson bracket, we can continue the derivation of governing equations by postulating that the Poisson bracket describes the time evolution. That is, we assume that the total energy  $E$  of the continuous body depends on the

<sup>5</sup>For details, see Pavelka et al. [2019].

<sup>6</sup>Note that if we write  $\partial AB$ , we mean  $\partial(A)B$ .

state variables and write  $\dot{A} = \{A, E\}^{(E)}$ . Furthermore, regrouping the terms and integrating by parts (dropping the surface terms) yields

$$\begin{aligned}\dot{A} = & \int A_\rho[-\partial_i(\rho E_{m_i})] + A_s[-\partial_i(s E_{m_i})] + A_{F_{iI}}[-E_{m_k}\partial_k F_{iI} + \partial_j E_{m_i} F_{jI}] \\ & + A_{m_i}[-\partial_j(m_i E_{m_j}) - \rho\partial_i E_\rho - m_j\partial_i E_{m_j} - s\partial_i E_s - F_{jJ}\partial_i E_{F_{jJ}} \\ & + \partial_j(F_{jI} E_{F_{iI}} - F_{iI} E_{F_{jI}})] d\mathbf{x}.\end{aligned}$$

Comparing this to directly computed

$$\dot{A} = \int A_\rho \frac{\partial \rho}{\partial t} + A_{m_i} \frac{\partial m_i}{\partial t} + A_s \frac{\partial s}{\partial t} + A_{F_{iI}} \frac{\partial F_{iI}}{\partial t} d\mathbf{x}$$

and using the fact  $A$  is arbitrary, one can derive<sup>7</sup>

$$\frac{\partial \rho}{\partial t} = -\partial_i(\rho E_{m_i}), \quad (1.1)$$

$$\begin{aligned}\frac{\partial m_i}{\partial t} = & -\partial_j(m_i E_{m_j}) - \rho\partial_i E_\rho - m_j\partial_i E_{m_j} - s\partial_i E_s - F_{jJ}\partial_i E_{F_{jJ}} \\ & + \partial_j(F_{jI} E_{F_{iI}} - F_{iI} E_{F_{jI}}),\end{aligned} \quad (1.2)$$

$$\frac{\partial s}{\partial t} = -\partial_i(s E_{m_i}), \quad (1.3)$$

$$\frac{\partial F_{iI}}{\partial t} = -E_{m_k}\partial_k F_{iI} + \partial_j E_{m_i} F_{jI}, \quad (1.4)$$

which are the desired governing equations.

However, these are not the only equations one may get. We may change the state variables by replacing the deformation gradient with either the left Cauchy-Green tensor  $\mathbb{B} = \mathbb{F}\mathbb{F}^\top$ , or the distortion matrix  $\mathbb{A} = \mathbb{F}^{-1}$ . We will study these options in the following sections.

## 1.4 Equations Involving the Left Cauchy-Green Tensor

The key step in the process of getting the governing equations involving  $\mathbb{B}$  is to project the Eulerian Poisson bracket from  $\mathbb{F}$  to  $\mathbb{B}$ . The rest of the derivation is very similar. Note that in this and the following section, we will use arbitrary functionals  $C$  and  $D$  instead of  $A$  and  $B$  to clearly distinguish them from the tensors  $\mathbb{A}$  and  $\mathbb{B}$ .

Before carrying out the actual projection, let us first compute a few important derivatives. Since  $B_{kl} = F_{kK} F_{lK}$ , one may write

$$\frac{\partial B_{kl}}{\partial F_{iI}} = \delta_{ik}\delta_{IK} F_{lK} + \delta_{li}\delta_{IK} F_{kK} = \delta_{ik} F_{lI} + \delta_{il} F_{kI}.$$

Let us now take arbitrary functional  $C(\rho, \mathbf{m}, s, \mathbb{B})$ , which can be taken as a functional  $C^1$  of  $\mathbb{F}$ , i.e.,  $C(\rho, \mathbf{m}, s, \mathbb{B}) = C^1(\rho, \mathbf{m}, s, \mathbb{F})$ . Then  $\frac{\delta C^1}{\delta \rho} = \frac{\delta C}{\delta \rho}$ ,  $\frac{\delta C^1}{\delta \mathbf{m}} = \frac{\delta C}{\delta \mathbf{m}}$ ,

---

<sup>7</sup>For details, see appendix A.2.

$\frac{\delta C^1}{\delta s} = \frac{\delta C}{\delta s}$  and

$$\begin{aligned}
\frac{\delta C^1}{\delta F_{iI}} &= \frac{\delta C}{\delta B_{kl}} \frac{\partial B_{kl}}{\partial F_{iI}} \\
&= \frac{\delta C}{\delta B_{kl}} (\delta_{ik} F_{lI} + \delta_{il} F_{kI}) \\
&= \frac{\delta C}{\delta B_{il}} F_{lI} + \frac{\delta C}{\delta B_{ki}} F_{kI} \\
&= \frac{\delta C}{\delta B_{il}} F_{lI} + \frac{\delta C}{\delta B_{li}} F_{lI}.
\end{aligned}$$

Omitting the upper index 1 for brevity, we now finally project the Poisson bracket:

$$\begin{aligned}
\{C, D\}^{(E)} &= \{C, D\}^{(FM)} + \int F_{jI} (C_{F_{iI}} \partial_j D_{m_i} - D_{F_{iI}} \partial_j C_{m_i}) d\mathbf{x} \\
&\quad - \int \partial_k F_{iI} (C_{F_{iI}} D_{m_k} - D_{F_{iI}} C_{m_k}) d\mathbf{x} \\
&= \{C, D\}^{(FM)} + \int F_{jI} [(C_{B_{il}} F_{lI} + C_{B_{li}} F_{lI}) \partial_j D_{m_i} \\
&\quad - (D_{B_{il}} F_{lI} + D_{B_{li}} F_{lI}) \partial_j C_{m_i}] d\mathbf{x} \\
&\quad - \int \partial_k F_{iI} [(C_{B_{il}} F_{lI} + C_{B_{li}} F_{lI}) D_{m_k} - (D_{B_{il}} F_{lI} + D_{B_{li}} F_{lI}) C_{m_k}] d\mathbf{x} \\
&= \{C, D\}^{(FM)} + \int C_{B_{il}} (B_{jl} \partial_j D_{m_i} + B_{ji} \partial_j D_{m_l}) \\
&\quad - D_{B_{il}} (B_{jl} \partial_j C_{m_i} + B_{ji} \partial_j C_{m_l}) d\mathbf{x} \\
&\quad - \int (C_{B_{il}} \partial_k F_{iI} F_{lI} + C_{B_{li}} \partial_k F_{iI} F_{lI}) D_{m_k} \\
&\quad - (D_{B_{il}} \partial_k F_{iI} F_{lI} + D_{B_{li}} \partial_k F_{iI} F_{lI}) C_{m_k} d\mathbf{x},
\end{aligned}$$

which yields

$$\begin{aligned}
\{C, D\}^{(E)} &= \{C, D\}^{(FM)} + \int C_{B_{il}} (B_{jl} \partial_j D_{m_i} + B_{ji} \partial_j D_{m_l}) \\
&\quad - D_{B_{il}} (B_{jl} \partial_j C_{m_i} + B_{ji} \partial_j C_{m_l}) d\mathbf{x} \\
&\quad - \int (C_{B_{il}} \partial_k F_{iI} F_{lI} + C_{B_{li}} \partial_k F_{iI} F_{lI}) D_{m_k} \\
&\quad - (D_{B_{il}} \partial_k F_{iI} F_{lI} + D_{B_{li}} \partial_k F_{iI} F_{lI}) C_{m_k} d\mathbf{x} \\
&= \{C, D\}^{(FM)} + \int C_{B_{il}} (B_{jl} \partial_j D_{m_i} + B_{ji} \partial_j D_{m_l}) \\
&\quad - D_{B_{il}} (B_{jl} \partial_j C_{m_i} + B_{ji} \partial_j C_{m_l}) d\mathbf{x} \\
&\quad - \int \partial_k B_{il} (C_{B_{il}} D_{m_k} - D_{B_{il}} C_{m_k}) d\mathbf{x}.
\end{aligned}$$

This defines the projected Poisson bracket:

$$\begin{aligned}
\{C, D\}^{(LCG)} &= \{C, D\}^{(FM)} + \int C_{B_{il}} (B_{jl} \partial_j D_{m_i} + B_{ji} \partial_j D_{m_l}) \\
&\quad - D_{B_{il}} (B_{jl} \partial_j C_{m_i} + B_{ji} \partial_j C_{m_l}) d\mathbf{x} \\
&\quad - \int \partial_k B_{il} (C_{B_{il}} D_{m_k} - D_{B_{il}} C_{m_k}) d\mathbf{x}.
\end{aligned}$$

Taking once again  $\{C, E\}^{(\text{LCG})}$ , integrating some terms by parts and comparing this to  $\dot{C}$  computed from the chain rule, one obtains

$$\frac{\partial \rho}{\partial t} = -\partial_i(\rho E_{m_i}), \quad (1.5)$$

$$\begin{aligned} \frac{\partial m_i}{\partial t} = & -\partial_j(m_i E_{m_j}) - \rho \partial_i E_\rho - m_j \partial_i E_{m_j} - s \partial_i E_s + \partial_i B_{jk} E_{B_{jk}} \\ & + \partial_j(B_{jk}(E_{B_{ik}} + E_{B_{ki}})), \end{aligned} \quad (1.6)$$

$$\frac{\partial s}{\partial t} = -\partial_i(s E_{m_i}), \quad (1.7)$$

$$\frac{\partial B_{ik}}{\partial t} = -E_{m_j} \partial_j B_{ik} + B_{jk} \partial_j E_{m_i} + B_{ji} \partial_j E_{m_k}. \quad (1.8)$$

Let us assume the energy to be in the form

$$E(\rho, \mathbf{m}, s, \mathbb{B}) = \int \frac{1}{2\rho} \mathbf{m}^2 + \varepsilon_1(\rho, s, \mathbb{B}) d\mathbf{x},$$

for instance the neo-Hookean energy  $E(\rho, \mathbf{m}, s, \mathbb{B}) = \int \frac{1}{2\rho} \mathbf{m}^2 + \rho \frac{\mu}{2} (\text{tr}(\mathbb{B}) - 3 - \ln(\det(\mathbb{B}))) d\mathbf{x}$ , where  $\mu$  is a constant. Then  $E_{m_j} = \frac{m_j}{\rho} = v_j$  and equation (1.8) gets the form

$$\overset{\nabla}{\mathbb{B}} = 0,$$

where  $\overset{\nabla}{\mathbb{B}}$  is the upper convected derivative of  $\mathbb{B}$ . This result corresponds to that of the standard approach.

Also note that equation (1.5) is the equation of continuity. Let us define the generalized pressure  $p_1$  by  $p_1 = -\varepsilon + \rho \varepsilon_\rho + s \varepsilon_s + \mathbf{m} \varepsilon_{\mathbf{m}}$ , where  $\varepsilon$  is the volume density of the total energy  $E$ . Then equation (1.6) gets the form

$$\frac{\partial m_i}{\partial t} + \partial_j(m_i E_{m_j}) = -\partial_i p + \partial_j(B_{jk}(E_{B_{ik}} + E_{B_{ki}})).$$

Further defining  $\tau_{ij} \stackrel{\text{def}}{=} B_{jk}(E_{B_{ik}} + E_{B_{ki}})$  we may finally rewrite equation (1.6) into the form

$$\partial_t \mathbf{m} + \text{div}(\mathbf{m} \otimes \mathbf{v}) = \text{div}(-p_1 \mathbb{I} + \tau),$$

that is, in the so called divergence form. This guarantees the momentum to be conserved.

In other words, the resulting equations are the same as in the classical approach, if we neglect the outer (volume) forces.<sup>8</sup> An important feature of this set of equations is that the stress tensor is uniquely determined once the energy is prescribed. That is, we do not need additional constitutive relations to describe it. Similar observations could, of course, be done about system (1.1) – (1.4), as is shown by Pavelka et al. [2019].

In chapter 3, we will analytically solve a few problems described by these equations. However, as stated in the introduction, we will be mostly interested in the equations involving the distortion matrix  $\mathbb{A}$ . Before that, however, we compare our results with the standard neo-Hookean solids.

---

<sup>8</sup>Outer forces are briefly addressed in section 2.4.

## 1.5 Comparison to neo-Hookean Solids

In the previous section, we have mentioned the neo-Hookean energy. A comparison of the model resulting from it and the neo-Hookean model derived from the balance equations and standard thermodynamic approach is of particular interest. To briefly recapitulate the standard approach, let us denote  $e_1 = \frac{\varepsilon_1}{\rho}$  and  $\varsigma = \frac{s}{\rho}$ . Then we assume  $e_1 = e_{\text{micro}}(\rho, \varsigma) + \frac{\mu}{2}(\text{tr}(\mathbb{B}) - 3 - \ln(\det(\mathbb{B})))$  and compute

$$\rho \dot{e}_1 = \rho \frac{\partial e_1}{\partial \varsigma} \dot{\varsigma} + \rho \frac{\partial e_1}{\partial \mathbb{B}} \dot{\mathbb{B}} + \rho \frac{\partial e_1}{\partial \rho} \dot{\rho}.$$

Now we define the temperature as  $T = \frac{\partial e_1}{\partial \varsigma}$  and  $\mathbb{D} = \frac{1}{2}(\mathbb{L} + \mathbb{L}^\top) = \frac{1}{2}(\nabla \mathbf{v} + (\nabla \mathbf{v})^\top)$ . We then recall  $\dot{\mathbb{B}} = \mathbb{L}\mathbb{B} + \mathbb{B}\mathbb{L}^\top$ ,  $\rho \dot{e}_1 = \mathbb{T} : \mathbb{D} - \text{div}(\mathbf{j}_e)$ , where  $\mathbf{j}_e$  is the heat flux. Finally, we assume  $\rho^2 \frac{\partial e_1}{\partial \rho} = p_1$ .<sup>9</sup> Now we can proceed as follows:

$$\begin{aligned} \rho T \dot{\varsigma} &= \mathbb{T} : \mathbb{D} - \text{div}(\mathbf{j}_e) - \rho \frac{\partial e_1}{\partial \mathbb{B}} (\mathbb{L}\mathbb{B} + \mathbb{B}\mathbb{L}^\top) + \rho^2 \frac{\partial e_1}{\partial \rho} \text{div}(\mathbf{v}) \\ &= \left( \mathbb{T} - 2\rho \frac{\partial e_1}{\partial \mathbb{B}} \mathbb{B} + p_1 \mathbb{I} \right) : \mathbb{D} - \text{div}(\mathbf{j}_e), \\ \rho \dot{\varsigma} + \text{div} \left( \frac{\mathbf{j}_e}{T} \right) &= \frac{1}{T} \left[ \left( \mathbb{T} - 2\rho \frac{\partial e_1}{\partial \mathbb{B}} \mathbb{B} + p_1 \mathbb{I} \right) : \mathbb{D} - \frac{\mathbf{j}_e \cdot \nabla T}{T} \right]. \end{aligned}$$

From this, assuming there is no dissipation, we get the constitutive relation

$$\mathbb{T} = -p_1 \mathbb{I} + 2\rho \frac{\partial e_1}{\partial \mathbb{B}} \mathbb{B}. \quad (1.9)$$

Next, we compute

$$\begin{aligned} \frac{\partial e_1}{\partial \mathbb{B}} &= \frac{\mu}{2} \frac{\partial (\text{tr}(\mathbb{B}) - 3 - \ln(\det(\mathbb{B})))}{\partial \mathbb{B}} \\ &= \frac{\mu}{2} \left( \mathbb{I} - \frac{1}{\det(\mathbb{B})} \frac{\partial \det(\mathbb{B})}{\partial \mathbb{B}} \right) \\ &= \frac{\mu}{2} (\mathbb{I} - \mathbb{B}^{-\top}). \end{aligned}$$

Plugging this into (1.9), we get

$$\mathbb{T} = -p_1 \mathbb{I} + \rho \mu (\mathbb{B} - \mathbb{I}), \quad (1.10)$$

which is the desired stress tensor.

Let us now focus on the stress tensor introduced in the previous section, using the already computed  $\frac{\partial e_1}{\partial \mathbb{B}}$  to our advantage. We start with the same energy  $e_1 = e_{\text{micro}}(\rho, \varsigma) + \frac{\mu}{2}(\text{tr}(\mathbb{B}) - 3 - \ln(\det(\mathbb{B})))$ . It is defined as

$$\begin{aligned} -p_1 \mathbb{I} + (E_{\mathbb{B}} + E_{\mathbb{B}}^\top) \mathbb{B} &= -p_1 \mathbb{I} + \frac{\rho \mu}{2} \left( (\mathbb{I} - \mathbb{B}^{-\top}) + (\mathbb{I} - \mathbb{B}^{-\top})^\top \right) \mathbb{B} \\ &= -p_1 \mathbb{I} + \rho \mu (\mathbb{B} - \mathbb{I}), \end{aligned}$$

which is the same stress tensor as (1.10). We thus conclude that a neo-Hookean model can be described by Hamiltonian mechanics. Furthermore, neglecting the microscale energy, we get the constitutive relation

$$\mathbb{T} = \rho \mu (\mathbb{B} - \mathbb{I}),$$

which we will use in the next chapter, and call it the neo-Hookean solid.

<sup>9</sup>This is actually true and can be proved in a similar way to that presented in section 1.7.

## 1.6 Equations Involving the Distortion Matrix

Following the procedure from the previous section, we need to change variables in the Eulerian Poisson bracket. Before actually doing so, let us once again compute a few derivatives. Since  $\mathbb{A} = \mathbb{F}^{-1}$ , we may write  $A_{Kk}F_{jK} = \delta_{kj}$ . Differentiating this equation with respect to  $F_{iI}$  and multiplying the result by  $A_{Jj}$ , we get

$$\begin{aligned} \left( \frac{\partial A_{Kk}}{\partial F_{iI}} F_{jK} + A_{kK} \frac{\partial F_{jK}}{\partial F_{iI}} \right) A_{Jj} &= 0, \\ \frac{\partial A_{Kk}}{\partial F_{iI}} \delta_{KJ} &= -A_{Kk} A_{Jj} \delta_{ij} \delta_{IK}, \\ \frac{\partial A_{Kk}}{\partial F_{iI}} \delta_{KJ} &= -A_{Ik} A_{Ji}, \\ \frac{\partial A_{Kk}}{\partial F_{iI}} &= -A_{Ik} A_{Ki}. \end{aligned}$$

Thus

$$\frac{\delta C}{\delta F_{iI}} = -\frac{\delta C}{\delta A_{Kk}} A_{Ik} A_{Ki}.$$

Moreover  $0 = \partial_k \delta_{ji} = \partial_k (A_{Ij} F_{iI}) = \partial_k A_{Ij} F_{iI} + A_{Ij} \partial_k F_{iI}$ . Therefore  $\partial_k A_{Ij} F_{iI} = -A_{Ij} \partial_k F_{iI}$  and

$$\begin{aligned} \{C, D\}^{(E)} &= \{C, D\}^{(FM)} + \int F_{jI} (C_{F_{iI}} \partial_j D_{m_i} - D_{F_{iI}} \partial_j C_{m_i}) d\mathbf{x} \\ &\quad - \int \partial_k F_{iI} (C_{F_{iI}} D_{m_k} - D_{F_{iI}} C_{m_k}) d\mathbf{x} \\ &= \{C, D\}^{(FM)} + \int F_{jI} (-C_{A_{Kk}} A_{Ik} A_{Ki} \partial_j D_{m_i} + D_{A_{Kk}} A_{Ik} A_{Ki} \partial_j C_{m_i}) d\mathbf{x} \\ &\quad - \int \partial_k F_{iI} (-C_{A_{Jj}} A_{Ij} A_{Ji} D_{m_k} + D_{A_{Jj}} A_{Ij} A_{Ji} C_{m_k}) d\mathbf{x} \\ &= \{C, D\}^{(FM)} - \int A_{Ki} \delta_{jk} (C_{A_{Kk}} \partial_j D_{m_i} - D_{A_{Kk}} \partial_j C_{m_i}) d\mathbf{x} \\ &\quad - \int \partial_k A_{Ij} F_{iI} A_{Ji} (C_{A_{Jj}} D_{m_k} - D_{A_{Jj}} C_{m_k}) d\mathbf{x} \\ &= \{C, D\}^{(FM)} - \int A_{Ki} (C_{A_{Kk}} \partial_k D_{m_i} - D_{A_{Kk}} \partial_k C_{m_i}) d\mathbf{x} \\ &\quad - \int \partial_k A_{Jj} (C_{A_{Jj}} D_{m_k} - D_{A_{Jj}} C_{m_k}) d\mathbf{x}. \end{aligned}$$

This defines the Poisson bracket:

$$\begin{aligned} \{C, D\}^{(A)} &= \{C, D\}^{(FM)} - \int A_{Ki} (C_{A_{Kk}} \partial_k D_{m_i} - D_{A_{Kk}} \partial_k C_{m_i}) d\mathbf{x} \\ &\quad - \int \partial_k A_{Jj} (C_{A_{Jj}} D_{m_k} - D_{A_{Jj}} C_{m_k}) d\mathbf{x}, \end{aligned}$$

which in turn generates the governing equations

$$\frac{\partial \rho}{\partial t} = -\partial_i(\rho E_{m_i}), \quad (1.11)$$

$$\begin{aligned} \frac{\partial m_i}{\partial t} = & -\partial_j(m_i E_{m_j}) - \rho \partial_i E_\rho - m_j \partial_i E_{m_j} - s \partial_i E_s \\ & + \partial_i A_{Ll} E_{A_{Ll}} - \partial_l(A_{Li} E_{A_{Ll}}), \end{aligned} \quad (1.12)$$

$$\frac{\partial s}{\partial t} = -\partial_i(s E_{m_i}), \quad (1.13)$$

$$\frac{\partial A_{Li}}{\partial t} = -\partial_l(A_{Li} E_{m_i}) + (\partial_l A_{Li} - \partial_i A_{Ll}) E_{m_i}. \quad (1.14)$$

This system was first introduced by Godunov [1961]. From now on, we will always equip these equations with the total energy in the following form:

$$E = \int \varepsilon(\rho, \mathbf{m}, s, \mathbb{A}) d\mathbf{x} = \int \varepsilon_{\text{kin}}(\rho, \mathbf{m}) + \varepsilon_1(\rho, s, \mathbb{A}) d\mathbf{x},$$

where  $\varepsilon_{\text{kin}} = \frac{1}{2\rho} \mathbf{m}^2$ . Then  $E_{m_i} = v_i$ . Furthermore, we assume  $\varepsilon_1$  to be in the form  $\varepsilon_1(\rho, s, \mathbb{A}) = \varepsilon_{\text{micro}}(\rho, s) + \varepsilon_{\text{meso}}(\rho, \mathbb{A})$ , where  $\varepsilon_{\text{meso}}(\rho, \mathbb{A}) = \rho \frac{c_s^2}{4} \|\text{dev}(\mathbb{G})\|_F$ . Here,  $\mathbb{G} = \mathbb{A}^T \mathbb{A}$ ,  $\text{dev}(\mathbb{G}) = \mathbb{G} - \frac{1}{3} \text{tr}(\mathbb{G}) \mathbb{I}$  and  $c_s$  is a material parameter for simplicity assumed to be constant. Thus, we have the energy in the form

$$E = \int \varepsilon_{\text{micro}}(\rho, s) + \frac{1}{2\rho} \mathbf{m}^2 + \rho \frac{c_s^2}{4} \|\text{dev}(\mathbb{G})\|_F d\mathbf{x}.$$

The usage of this energy is justified by Dumbser et al. [2016]. The energy  $\varepsilon_{\text{micro}}$  should capture the energy at the scale of particles, while  $\varepsilon_{\text{meso}}$  stores the energy of the deformation.

We further show that (1.14) gives the same results as time evolution for  $\mathbb{A}$  from classical approach. In the classical approach, we assume  $\mathbb{F}^1$  and  $\mathbb{A}^1$  to be  $\mathbb{F}$  and  $\mathbb{A}$  expressed in Lagrangian coordinates respectively, i.e.,  $\mathbb{F}^1(\mathbf{X}, t) = \mathbb{F}(\mathbf{x}(\mathbf{X}, t), t)$  and  $\mathbb{A}^1(\mathbf{X}, t) = \mathbb{A}(\mathbf{x}(\mathbf{X}, t), t)$ , then  $\frac{\partial \mathbb{F}^1}{\partial t} = \frac{d\mathbb{F}}{dt}$  and  $\frac{\partial \mathbb{A}^1}{\partial t} = \frac{d\mathbb{A}}{dt}$ . Thus, differentiating  $\mathbb{F}^1 \mathbb{A}^1 = \mathbb{I}$  over time, we obtain

$$\begin{aligned} \mathbb{F}^1 \frac{\partial \mathbb{A}^1}{\partial t} &= -\frac{\partial \mathbb{F}^1}{\partial t} \mathbb{A}^1 \\ \mathbb{F}^1 \frac{\partial \mathbb{A}^1}{\partial t} &= -\mathbb{L} \mathbb{F}^1 \mathbb{A}^1 \\ \frac{\partial \mathbb{A}^1}{\partial t} &= -\mathbb{A}^1 \mathbb{L} \\ \frac{d\mathbb{A}}{dt} &= \mathbb{A} \mathbb{L}, \end{aligned}$$

where  $\mathbb{L} = \frac{\partial \mathbf{v}}{\partial \mathbf{x}}$  is the velocity gradient. This is indeed only a rewritten form of (1.14).

Moreover, we focus on equation (1.12). Defining the pressure  $p = -\varepsilon + \rho \varepsilon_\rho + m_j \varepsilon_{m_j} + s \varepsilon_s$  and

$$\sigma_{il} = -(A_{Li} E_{A_{Ll}}), \quad (1.15)$$

it gets the divergence form

$$\partial_t \mathbf{m} + \operatorname{div}(\mathbf{m} \otimes \mathbf{v}) = \operatorname{div}(-p\mathbb{I} + \sigma).$$

We have already shown that the stress tensor for the model with left Cauchy-Green tensor can describe the neo-Hookean solid. An interesting exercise on tensor calculus is to show the same holds for the model with distortion matrix as well; see appendix A.3.

Finally, we observe that total entropy, i.e., the volume integral of  $s$  and the total energy  $E$  are preserved. Entropy does not change since  $s$  is modelled by the same equation as  $\rho$  describing no change in mass. This demonstrates the facts that equations (1.11) – (1.14) model the reversible part of continuum mechanics. The energy is preserved from antisymmetry of the Poisson bracket. Namely:

$$\dot{E} = \{E, E\}^{(A)} = -\{E, E\}^{(A)},$$

which implies  $\dot{E} = 0$ . This is, however, true only in the interior of the body. The absolute energy can grow as a consequence of forces on the boundary, as we will show in section 3.1.

We thus conclude that even the set of equations (1.11) – (1.14) is compatible with the classical approach.

## 1.7 Properties of the Pressure

We have defined the pressure in the previous section. However, from the definition provided, it is vastly unclear, what physical meaning the quantity has. We therefore try to express the pressure in a different way. Let us first substitute  $\varepsilon$  with  $\varepsilon_{\text{kin}} + \varepsilon_1$  in the definition, producing<sup>10</sup>

$$\begin{aligned} p &= -\varepsilon_1 + \rho\varepsilon_\rho^1 + m_j\varepsilon_{m_j}^1 + s\varepsilon_s^1 - \varepsilon_{\text{kin}} + \rho\varepsilon_\rho^{\text{kin}} + m_j\varepsilon_{m_j}^{\text{kin}} + s\varepsilon_s^{\text{kin}} \\ &= -\varepsilon_1 + \rho\varepsilon_\rho^1 + m_j\varepsilon_{m_j}^1 + s\varepsilon_s^1 - \frac{1}{2\rho}\mathbf{m}^2 + \rho\frac{-1}{\rho^2}\mathbf{m}^2 + \mathbf{m}\frac{1}{\rho}\mathbf{m} \\ &= -\varepsilon_1 + \rho\varepsilon_\rho^1 + m_j\varepsilon_{m_j}^1 + s\varepsilon_s^1 \\ &= -\varepsilon_1 + \rho\varepsilon_\rho^1 + s\varepsilon_s^1. \end{aligned}$$

We recall  $T = \left(\frac{\partial e_1}{\partial \varsigma}\right)_\rho$  and compute

$$\left(\frac{\partial \varepsilon_1}{\partial s}\right)_{\rho, \mathbb{A}} = \left(\frac{\partial(\rho e_1)}{\partial s}\right)_{\rho, \mathbb{A}} = \rho \left(\frac{\partial e_1}{\partial \varsigma}\right)_{\rho, \mathbb{A}} \frac{\partial \varsigma}{\partial s} = \rho T \frac{1}{\rho} = T.$$

Moreover, we define  $\eta = \varepsilon_\rho^1$ . Then:

$$\begin{aligned} p &= -\varepsilon_1 + sT + \rho\eta, \\ \frac{p}{\rho} &= -e_1 + \varsigma T + \eta. \end{aligned} \tag{1.16}$$

<sup>10</sup>Where needed, the lower index 1 is shifted up to avoid collisions with other indices.

Now, we stress that

$$e_1(\rho, \varsigma, \mathbb{A}) = \frac{\varepsilon_1(\rho, \rho\varsigma, \mathbb{A})}{\rho},$$

which, altogether with (1.16), yields:

$$\begin{aligned} \left( \frac{\partial e_1}{\partial \rho} \right)_{\varsigma, \mathbb{A}} &= \frac{\rho \left( \frac{\partial \varepsilon_1}{\partial \rho} + \frac{\partial \varepsilon_1}{\partial s} \varsigma \right) - \varepsilon_1}{\rho^2} \\ &= \frac{\frac{\partial \varepsilon_1}{\partial \rho} + \frac{\partial \varepsilon_1}{\partial s} \varsigma - e_1}{\rho} \\ &= \frac{-e_1 + T\varsigma + \eta}{\rho} \\ &= \frac{p}{\rho^2}. \end{aligned}$$

Thus

$$p = \rho^2 \left( \frac{\partial e_1}{\partial \rho} \right)_{\varsigma, \mathbb{A}}. \quad (1.17)$$

Further recalling that  $e_{\text{meso}} = \frac{\varepsilon_{\text{meso}}}{\rho}$  does not depend on  $\rho$ , we obtain that (1.17) gets the form

$$p = \rho^2 \left( \frac{\partial e_{\text{micro}}}{\partial \rho} \right)_{\varsigma}. \quad (1.18)$$

This definition of the pressure is compatible with standard thermodynamics and is often used in the formulation of model (1.11) – (1.14).

## 2. Thermodynamics

### 2.1 Addition of Dissipation

The systems introduced in the previous chapter model reversible evolution only. To include the dissipation into system (1.11) – (1.14), we add algebraic source terms into the right hand sides of the equations, in the form summarized by Jackson [2018]. Let us first define  $\Psi = \frac{\partial e}{\partial \mathbb{A}}$ . Then, simplifying the notion, we get the SHTC model with dissipation in the form

$$\frac{\partial \rho}{\partial t} + \frac{\partial(\rho v_i)}{\partial x_i} = 0, \quad (2.1)$$

$$\frac{\partial m_i}{\partial t} + \frac{\partial(m_i v_j + \rho p \delta_{ij} - \sigma_{ij})}{\partial x_j} = 0, \quad (2.2)$$

$$\frac{\partial s}{\partial t} + \frac{\partial(sv_i)}{\partial x_i} = \frac{\rho}{T} \frac{\Psi_{kl} \Psi_{kl}}{\theta}, \quad (2.3)$$

$$\frac{\partial A_{Ll}}{\partial t} + \frac{\partial(A_{Li} v_i)}{\partial x_i} + v_i \left( \frac{\partial A_{Li}}{\partial x_l} - \frac{\partial A_{Ll}}{\partial x_i} \right) = -\frac{\Psi_{Ll}}{\theta}. \quad (2.4)$$

The following forms are used:

$$\theta = \frac{\tau_1 c_s^2}{3|\mathbb{A}|^{5/3}}$$

$$\tau_1 = \begin{cases} \frac{6\mu}{\rho_0 c_s^2} & \text{viscous fluids} \\ \tau_0 \left( \frac{\sigma_0}{\|\text{dev}(\sigma)\|_F} \right)^n & \text{elastoplastic solids} \end{cases}$$

where the quantities  $\mu, \tau_0, \sigma_0$  and  $n$  are material parameters defining the dissipation.

The choice of such dissipation is justified by Dumbser et al. [2016]. In the following sections, we will show that this dissipation is, in fact, generated by a quadratic dissipation potential. Before doing so, let us comment on system (2.1) – (2.4).

Firstly, since we choose material parameters in such a way, that  $\theta > 0$  and since  $\rho, T > 0$ , the dissipative term for entropy density is non-negative, thus producing entropy. This is a desired quality of dissipation.

Secondly, the distortion matrix  $\mathbb{A}$  has been introduced as the inverse of the deformation gradient. Under the assumption that the motion is smooth, the second partial derivatives with respect to space are interchangeable. This should also be true for the inverse mapping from the actual configuration to the reference one. Thus,

$$\text{curl}(\mathbb{A}) = \begin{pmatrix} \text{curl}(\mathbf{A}_1) \\ \text{curl}(\mathbf{A}_2) \\ \text{curl}(\mathbf{A}_3) \end{pmatrix} = 0,$$

where  $\mathbf{A}_1$ ,  $\mathbf{A}_2$  and  $\mathbf{A}_3$  are the rows of  $\mathbb{A}$ .

However, after the dissipation is added, this property do not have to be valid, as we will show in chapter 3. If  $\text{curl}(\mathbb{A}) \neq 0$ , the second derivatives are not interchangeable and thus integration of  $\mathbb{A}$  depends on the integration path. Thus, the actual configuration cannot be reconstructed from the reference configuration by integrating  $\mathbb{A}^{-1}$ . Moreover  $\text{curl}(\mathbb{A})$ , also called the Burgers tensor, describes the dislocations. Its evolution describes the dynamics of dislocations. A reader interested in the topic of dislocations is recommended to see Landau and Lifshitz [1970].

In the case  $\text{curl}(\mathbb{A}) = 0$ , the integration of  $\mathbb{A}$  over its domain is possible and gives unique results. However, it does not have to constitute the actual global link between the two configurations, as we will demonstrate in chapter 3. Thus, after addition of dissipation, the distortion matrix must not be viewed as the inverse of the deformation gradient, but only as a matrix present in the equations.

## 2.2 Fundamental Relation

Let us denote  $\xi = (\rho, \mathbf{m}, \mathbb{A})$ . Then, throughout all of this text, we assume

$$\varepsilon = \varepsilon(\xi, s).$$

Moreover, we assume that the dependency on  $s$  is algebraic, i.e.,  $\varepsilon(\mathbf{x})$  depends on  $s(\mathbf{x})$  only. Since

$$\frac{\partial \varepsilon}{\partial s} = T > 0,$$

we have also that

$$s = s(\xi, \varepsilon),$$

actually. If we work with  $s = s(\xi, \varepsilon)$ , we talk about entropic representation. If, on the other hand, we work with  $\varepsilon = \varepsilon(\xi, s)$ , we call it the energetic representation. We denote the vector of all state variables by  $\mathbf{q}$ . This means  $\mathbf{q} = (\xi, s)$  or  $\mathbf{q} = (\xi, \varepsilon)$ , depending on the representation we work with.

Furthermore, denoting  $S = \int s d\mathbf{x}$  and  $E = \int \varepsilon d\mathbf{x}$ , it holds

$$\frac{\partial \varepsilon}{\partial s} = \left( \frac{\partial s}{\partial \varepsilon} \right)^{-1}, \quad \frac{\delta E}{\delta s} = \left( \frac{\delta S}{\delta \varepsilon} \right)^{-1}, \quad (2.5)$$

$$\frac{\delta E}{\delta \xi_i} = -\frac{\frac{\partial s}{\partial \xi_i}}{\frac{\partial s}{\partial \varepsilon}} = -\frac{\partial s}{\partial \xi_i} \frac{\partial \varepsilon}{\partial s}, \quad \frac{\delta S}{\delta \xi_i} = -\frac{\partial \varepsilon}{\partial \xi_i} \frac{\partial s}{\partial \varepsilon}. \quad (2.6)$$

These relations enable us to switch from one representation to the other.

## 2.3 Dissipation Potential

Let us now work within the entropic representation for a while. The derivatives of entropy with respect to state variables are called the conjugate variables and we denote them by asterisk, that is

$$\mathbf{q}^* = \frac{\delta S}{\delta \mathbf{q}}.$$

Then, according to Pavelka et al. [2018], the irreversible evolution of state variables is given by

$$(\dot{\mathbf{q}})_{\text{irr}} = \frac{\delta \Xi}{\delta \mathbf{q}^*} \Big|_{\mathbf{q}^* = S_{\mathbf{q}}}, \quad (2.7)$$

where the dissipation potential  $\Xi(\mathbf{q}^*)$  is a suitable functional of the conjugate variables. An example of such functional, perhaps most often used, is the quadratic one,

$$\Xi = \int \frac{1}{2} \mathbf{q}_i^* M_{ij} \mathbf{q}_j^* d\mathbf{x}, \quad (2.8)$$

where the matrix  $\mathbb{M}$  is called the dissipative matrix and is required to be symmetric and positive semi-definite, see Pavelka et al. [2018]. The irreversible evolution (2.7) of state variables then becomes

$$(\dot{q}_i)_{\text{irr}} = M_{ij} q_j^* \Big|_{\mathbf{q}^* = S_{\mathbf{q}}}.$$

From now on, let us assume that  $\Xi$  does not depend on  $\varepsilon^*$ . Moreover, we switch to the energetic representation, where the conjugate variables are denoted by a dagger, i.e.,

$$\mathbf{q}^\dagger = \frac{\delta E}{\delta \mathbf{q}}.$$

This notation enables us to rewrite (2.5), (2.6) to

$$s^\dagger = (\varepsilon^*)^{-1}, \quad \xi_j^\dagger = -\frac{\xi_j^*}{\varepsilon^*}. \quad (2.9)$$

Differentiation of these relations yields

$$\left( \frac{\partial \xi_i^\dagger}{\partial \xi_j^*} \right)_{\varepsilon^*} = -\frac{\delta_{ij}}{\varepsilon^*} = -\delta_{ij} s^\dagger, \quad \left( \frac{\partial s^\dagger}{\partial \xi_i^\dagger} \right)_{\varepsilon^*} = 0,$$

which lead us to

$$\begin{aligned} \left( \frac{\delta \Xi}{\delta \xi_i^*} \right)_{\varepsilon^*} &= \left( \frac{\delta \Xi}{\delta \xi_j^\dagger} \right)_{s^\dagger} \left( \frac{\partial \xi_j^\dagger}{\partial \xi_i^*} \right)_{\varepsilon^*} + \left( \frac{\delta \Xi}{\delta \xi_i^\dagger} \right)_{s^\dagger} \left( \frac{\partial s^\dagger}{\partial \xi_i^*} \right)_{\varepsilon^*} \\ &= -s^\dagger \left( \frac{\delta \Xi}{\delta \xi_i^\dagger} \right)_{s^\dagger}. \end{aligned} \quad (2.10)$$

Moreover the assumption that  $\Xi$  does not depend on  $\varepsilon^*$  implies that

$$(\dot{\varepsilon})_{\text{irr}} = \left( \frac{\delta \Xi}{\delta \varepsilon^*} \right)_{\xi^*} = 0, \quad (2.11)$$

which means that the energy stays conserved. Now, using (2.7), (2.10) and (2.11), we compute

$$(\dot{\xi}_i)_{\text{irr}} = \frac{\delta \Xi}{\delta \xi_i^*} \Big|_{\xi^* = S_\xi} = -s^\dagger \left( \frac{\delta \Xi}{\delta \xi_i^\dagger} \right)_{s^\dagger} \quad (2.12)$$

and

$$\begin{aligned}
(\dot{s})_{\text{irr}} &= \left( \frac{\partial s}{\partial \xi_i} \right)_{\varepsilon} (\dot{\xi}_i)_{\text{irr}} + \left( \frac{\partial s}{\partial \varepsilon} \right)_{\xi} (\dot{\varepsilon})_{\text{irr}} \\
&= \xi_i^* \left( \frac{\delta \Xi}{\delta \xi_i^*} \right)_{\varepsilon^*} + 0 = \xi_i^* (-s) \left( \frac{\delta \Xi}{\delta \xi_i^\dagger} \right)_{s^\dagger} = \xi_i^\dagger \left( \frac{\delta \Xi}{\delta \xi_i^\dagger} \right)_{s^\dagger}.
\end{aligned} \tag{2.13}$$

Next, we plug in the quadratic potential (2.8) into (2.12), (2.13). To do that, using (2.9), we compute

$$\Xi = \int \frac{1}{2} \mathbf{q}_i^* M_{ij} \mathbf{q}_j^* d\mathbf{x} = \int \frac{1}{2} \frac{\xi_i^\dagger}{s^\dagger} M_{ij} \frac{\xi_j^\dagger}{s^\dagger} d\mathbf{x},$$

for which we have:

$$\frac{\delta \Xi}{\delta \xi_i^\dagger} = M_{ij} \frac{\xi_j^\dagger}{(s^\dagger)^2}.$$

This leads to

$$(\dot{\xi}_i)_{\text{irr}} = -M_{ij} \frac{\xi_j^\dagger}{s^\dagger} = -M_{ij} \frac{\varepsilon_{\xi_j}}{\varepsilon_s}, \tag{2.14}$$

$$(\dot{s})_{\text{irr}} = \xi_i^\dagger M_{ij} \frac{\xi_j^\dagger}{s^\dagger} = \frac{1}{(\varepsilon_s)^2} \varepsilon_{\xi_i} M_{ij} \varepsilon_{\xi_j}. \tag{2.15}$$

From this and the positive semi-definiteness of  $\mathbb{M}$  we easily see that the irreversible evolution for dissipation is non-negative. In the case of a more general dissipation potential, this follows from the required convexity of  $\Xi$ . This fact is commented by Pavelka et al. [2018].

Finally, the specific form of the dissipation potential

$$\Xi = \int \frac{1}{2\rho\theta S_\varepsilon} \mathbb{A}^* : \mathbb{A}^* d\mathbf{x}$$

produces the very same dissipation as the one specified in section 2.1. To do that, we have chosen

$$\mathbb{M} = \frac{1}{\rho\theta S_\varepsilon} \tilde{\mathbb{I}},$$

where  $\tilde{\mathbb{I}}$  is a diagonal matrix with ones at indexes corresponding to  $\mathbb{A}^*$  and zeroes elsewhere.

## 2.4 Final Form of the Governing Equations

In this section, we will finalize the form of the equations we use. First of all, let us realize that system (2.1) – (2.4) is also equipped with the balance equation for energy. To derive it, we employ the chain rule and the governing equations:

$$\begin{aligned}
\frac{\partial \varepsilon}{\partial t} &= \frac{\partial \varepsilon}{\partial \rho} \frac{\partial \rho}{\partial t} + \frac{\partial \varepsilon}{\partial m_i} \frac{\partial m_i}{\partial t} + \frac{\partial \varepsilon}{\partial s} \frac{\partial s}{\partial t} + \frac{\partial \varepsilon}{\partial A_{Ll}} \frac{\partial A_{Ll}}{\partial t} \\
&= -\frac{\partial \varepsilon}{\partial \rho} \frac{\partial(\rho v_k)}{\partial x_k} - \frac{\partial \varepsilon}{\partial m_i} \frac{\partial(m_i v_k + p \delta_{ik} - \sigma_{ik})}{\partial x_k} - \frac{\partial \varepsilon}{\partial s} \frac{\partial(sv_k)}{\partial x_k} \\
&\quad - \frac{\partial \varepsilon}{\partial A_{Ll}} \left( \frac{\partial(A_{Lk} v_k)}{\partial x_l} + v_k \left( \frac{\partial A_{Ll}}{\partial x_k} - \frac{\partial A_{Lk}}{\partial x_l} \right) \right) \\
&= -\frac{\partial \varepsilon}{\partial \rho} \frac{\partial \rho}{\partial x_k} v_k - \rho \varepsilon_\rho \frac{\partial v_k}{\partial x_k} - \frac{\partial \varepsilon}{\partial m_i} \frac{\partial m_i}{\partial x_k} v_k - m_i \varepsilon_{m_i} \frac{\partial v_k}{\partial x_k} - \frac{\partial \varepsilon}{\partial m_i} \frac{\partial(p \delta_{ik} - \sigma_{ik})}{\partial x_k} \\
&\quad - \frac{\partial \varepsilon}{\partial s} \frac{\partial s}{\partial x_k} v_k - s \varepsilon_s \frac{\partial v_k}{\partial x_k} - \frac{\partial \varepsilon}{\partial A_{Ll}} \frac{\partial A_{Ll}}{\partial x_l} v_k - \frac{\partial \varepsilon}{\partial A_{Ll}} \left( \frac{\partial(A_{Lk} v_k)}{\partial x_l} - v_k \frac{\partial A_{Lk}}{\partial x_l} \right) \\
&= -\frac{\partial \varepsilon}{\partial x_k} v_k - (p + \varepsilon) \frac{\partial v_k}{\partial x_k} - \frac{\partial \varepsilon}{\partial A_{Ll}} \frac{\partial v_k}{\partial x_l} A_{Lk} - v_i \frac{\partial(p + \delta_{ik} - \sigma_{ik})}{\partial x_k} \\
&= -\frac{\partial \varepsilon}{\partial x_k} v_k - \varepsilon \frac{\partial v_k}{\partial x_k} - \frac{\partial v_i}{\partial x_k} (p \delta_{ik} - \sigma_{ik}) - v_i \frac{\partial(p \delta_{ik} - \sigma_{ik})}{\partial x_k} \\
&= -\frac{\partial(\varepsilon v_k + (p \delta_{ik} - \sigma_{ik}) v_i)}{\partial x_k}.
\end{aligned}$$

Thus

$$\frac{\partial \varepsilon}{\partial t} + \frac{\partial(\varepsilon v_k + (p \delta_{ik} - \sigma_{ik}) v_i)}{\partial x_k} = 0. \quad (2.16)$$

Equation (2.16) can be rewritten as

$$\frac{\partial \varepsilon}{\partial t} + \operatorname{div}(\varepsilon \mathbf{v}) = \operatorname{div}((-p \mathbb{I} + \sigma) \mathbf{v}),$$

which is the energy balance without volume forces, heat fluxes and heat sources.

Note that we have used the elastic equations without dissipative terms. However, these terms cancel out. This is either obvious from their construction from dissipation potential or by directly computing

$$\frac{\partial \varepsilon}{\partial A_{Ll}} \frac{\Psi_{Ll}}{\theta} - \frac{\partial \varepsilon}{\partial s} \frac{\rho}{T} \frac{\Psi_{kl} \Psi_{kl}}{\theta} = \frac{\rho \Psi_{Ll} \Psi_{Ll}}{\theta} - T \frac{\rho}{T} \frac{\Psi_{kl} \Psi_{kl}}{\theta} = 0.$$

We will use system (2.1) - (2.4) in analytic computations, while in numerical simulations, equation (2.3) will be replaced by (2.16).

Let us now assume we want to add a volume force, the density per mass of which is given by vector  $\mathbf{f}$ . Further let us assume  $\phi(\mathbf{x})$  is its potential, i.e.,  $\mathbf{f} = -\nabla \phi$ . We define new energy  $\tilde{\varepsilon} = \varepsilon + \rho \phi$ . The only term changed in system (2.1) - (2.4) is  $\rho \tilde{\varepsilon}_\rho$ , which produces an additional term  $-\rho(\nabla \phi)_i = \rho f_i$  to the right hand side of (2.2). Furthermore, this additional term adds  $\rho \mathbf{v} \mathbf{f}$  to the right hand side of the balance of energy. These results correspond to the standard approach to volume forces. However, we do not work with volume forces in this text.

The last thing needed to close the system is the specification of  $e_{\text{micro}}$ . In this

text, we assume it is in the Mie-Gruneisen form<sup>1</sup>, i.e., it can be expressed as

$$e_{\text{micro}}(\rho, p) = e^{\text{ref}}(\rho) + \frac{p - p^{\text{ref}}(\rho)}{\rho\Gamma(\rho)},$$

$$T = T^{\text{ref}} \exp\left(\int_{\rho_0}^{\rho} \frac{\Gamma(\tilde{\rho})}{\tilde{\rho}} d\tilde{\rho}\right) + \frac{e - e^{\text{ref}}}{c_v}$$

where

$$p^{\text{ref}}(\rho) = 0,$$

$$e^{\text{ref}}(\rho) = 0,$$

$$\Gamma(\rho) = \gamma - 1,$$

for an ideal gas or

$$p^{\text{ref}}(\rho) = \frac{c_0^2 \left(\frac{1}{\rho_0} - \frac{1}{\rho}\right)}{\left(\frac{1}{\rho_0} - u \left(\frac{1}{\rho_0} - \frac{1}{\rho}\right)\right)^2},$$

$$e^{\text{ref}}(\rho) = \frac{p^{\text{ref}}(\rho)}{2} \left(\frac{1}{\rho_0} - \frac{1}{\rho}\right),$$

$$\Gamma(\rho) = \Gamma_0 \frac{\rho_0}{\rho},$$

for the Shock Mie-Gruneisen equation of state. Here,  $\gamma$ ,  $c_0$ ,  $u$ ,  $\Gamma_0$  and  $c_v$  are some material parameters. The specification of common parameters used for numerical simulations is provided by tables A.1, A.2 and A.3 in appendix A.5. Note that the elastic parameters used for a solid describe copper, as stated by Jackson [2018].

---

<sup>1</sup>Mie-Gruneisen equation of state is described by Menikoff [2016].

# 3. Examples

## 3.1 Neo-Hookean Solid in One Dimension

Let us first assume we have a one-dimensional motion of a neo-Hookean solid. System (1.5) – (1.8) reduces to

$$\begin{aligned}\frac{\partial \rho}{\partial t} &= -\partial_x(\rho v), \\ \frac{\partial s}{\partial t} &= -\partial_x(sv), \\ \frac{\partial A}{\partial t} &= -\partial_x(Av), \\ \frac{\partial m}{\partial t} &= -\partial_x(mv) - \rho \partial_x(E_\rho) - m \partial_x(E_m) - s \partial_x(E_s) - A \partial_x(E_A)\end{aligned}$$

and the energy to  $E = \int \frac{m^2}{2\rho} + \rho \frac{\mu}{2}(B - 1 - \ln(B))$ . Here,  $A$  and  $B$  are the tensors, that we treat as numbers. Thus,  $\text{tr}(B) = \det(B) = B$ . Next, we assume the motion is described by a function  $x = x(X, t)$ . We compute

$$\begin{aligned}E_m &= v, \\ E_\rho &= -\frac{1}{2}v^2 + \frac{\mu}{2}(B - 1 - \ln(B)), \\ E_s &= 0, \\ E_A &= -\rho\mu(x_X^3 - x_X).\end{aligned}$$

We now assume  $\rho(X, 0) = \rho_0 = \text{const.}$  and recall  $\rho = \frac{\rho_0}{\det F} = \frac{\rho_0}{x_X}$ . As  $A$  and  $s$  are governed by the same equation, assuming  $A_0, s_0$  are constant, we get the solutions  $A = \frac{A_0}{x_X}, s = \frac{s_0}{x_X}$ , respectively. Let us now plug the above values into the balance of momentum and subtract the balance of mass, to get

$$\begin{aligned}\rho_t v + \rho v_t = m_t &= -\partial_x(mv) + \frac{1}{2}\rho \partial_x(v^2) - \rho \frac{\mu}{2} \partial_x(B - 1 - \ln(B)) - m \partial_x v - s \cdot 0 \\ &\quad + A \partial_x(\rho\mu(x_X^3 + x)), \\ \rho v_t &= -mv_x - \rho \frac{\mu}{2} \partial_x(x_X^2 - \ln(x_X^2)) + x_X^{-1} \partial_x(\rho\mu(x_X^3 + x)) \\ &= -mv_x - \rho \frac{\mu}{2} \partial_x(x_X^2 - \ln(x_X^2)) + x_X^{-1} \rho_0 \mu \partial_x \left( \frac{1}{x_X}(x_X^3 + x) \right) \\ &= -mv_x - \rho \frac{\mu}{2} \partial_x(x_X^2 - \ln(x_X^2)) + x_X^{-1} \rho_0 \mu \partial_x(x_X^2) \\ &= -mv_x + \rho \frac{\mu}{2} \partial_x(x_X^2) + \rho \frac{\mu}{2} \frac{1}{x_X^2} \partial_x(x_X^2) \\ &= -mv_x + \rho \frac{\mu}{2} \left( 1 + \frac{1}{x_X^2} \right) 2x_X \partial_x(x_X) \\ &= -mv_x + \rho\mu \left( 1 + \frac{1}{x_X^2} \right) x_X x_{XX} \frac{\partial X}{\partial x},\end{aligned}$$

which implies

$$v_t = -vv_x + \mu \left( 1 + \frac{1}{x_X^2} \right) x_X x_{XX} \frac{\partial X}{\partial x}. \quad (3.1)$$

If we assume that  $x_{XX} = 0$ , i.e.,

$$x(X, t) = C_1(t)X + C_2(t), \quad (3.2)$$

equation (3.1) reduces to  $v_t = -vv_x$ . Assuming linear velocity profile at  $t = 0$ , that is,  $v_0 = Cx$ , the method of characteristics gives

$$\begin{aligned} v(x, t) &= C(x - v(x, t)t) \\ (1 + Ct)v(x, t) &= Cx \\ v(x, t) &= \frac{Cx}{1 + Ct}. \end{aligned} \quad (3.3)$$

From (3.2), we have

$$\begin{aligned} v(x, t) &= C'_1(t)X(x, t) + C'_2(t) \\ &= \frac{C'_1(t)}{C_1(t)}(x - C_2(t)) + C'_2(t). \end{aligned}$$

Comparing this, to (3.3), one has  $\frac{C'_1(t)}{C_1(t)} = \frac{C}{1+Ct}$  and  $-\frac{C'_1(t)}{C_1(t)}C_2(t) + C'_2(t) = 0$ , from which we get  $C_1(t) = K_1(1 + Ct)$  and  $C_2(t) = K_2(1 + Ct)$ . Choosing  $K_1 = 1$  and  $K_2 = 0$ , we have found an analytical solution

$$x = (1 + Ct)X \quad (3.4)$$

to the Cauchy problem.

If we, however, restrict ourselves to  $X \in [-1, 1]$  and prescribe the boundary conditions as  $x(\pm 1, t) = \pm(1 + Ct)$ , solution (3.4) becomes a solution to a Dirichlet problem. This can be viewed as linear stretching (or shrinking) of a spring due to some forces on the edges of the spring. We now compute the energy of the spring as

$$\begin{aligned} E(t) &= \int_{-(1+Ct)}^{1+Ct} \frac{m^2}{2\rho} + \rho \frac{\mu}{2} (B - 1 - \ln(B)) dx \\ &= \int_{-(1+Ct)}^{1+Ct} \frac{\rho_0/2}{1 + Ct} \frac{C^2 x^2}{(1 + Ct)^2} + \frac{\rho_0}{1 + Ct} \frac{\mu}{2} \left( (1 + Ct)^2 - 1 - \ln \left( (1 + Ct)^2 \right) \right) dx \\ &= \left[ \frac{\rho_0 C^2}{6 \cdot (1 + Ct)^3} x^3 \right]_{-(1+Ct)}^{1+Ct} + \\ &\quad \left[ \frac{\rho_0}{1 + Ct} \frac{\mu}{2} \left( (1 + Ct)^2 - 1 - \ln \left( (1 + Ct)^2 \right) \right) x \right]_{-(1+Ct)}^{1+Ct} \\ &= \frac{\rho_0 C^2}{3} + \rho_0 \mu \left( (1 + Ct)^2 - 1 - \ln \left( (1 + Ct)^2 \right) \right). \end{aligned}$$

Thus, the kinetic energy does not change with time and because  $f(x) = x - \ln(x)$  is decreasing on  $(0, 1)$  and increasing on  $(1, \infty)$ , the total energy increases with time regardless of the sign of  $C$ .<sup>1</sup> This is an example of the fact that the energy can grow because of the forces on the boundary.

---

<sup>1</sup>Note however, that the solution has sense only for time  $t < \frac{1}{-C}$  if  $C < 0$ .

## 3.2 Vertical Vibrations under the neo-Hookean Model

Let us now assume a two dimensional infinite body under a deformation in the form

$$\begin{pmatrix} x \\ y \end{pmatrix} = \begin{pmatrix} X \\ Y + \psi(X, t) \end{pmatrix},$$

where  $\psi$  is smooth. We describe the motion by system (1.5) – (1.8) with the neo-Hookean energy, i.e., its two-dimensional reduction  $E = \int \frac{1}{2\rho} \mathbf{m}^2 + \rho \frac{\mu}{2} (\text{tr}(\mathbb{B}) - 2 - \ln(\det(\mathbb{B}))) dx$ . Further, we assume  $\rho_0$  and  $s_0$  to be constant.

One may easily compute

$$\begin{aligned} \mathbb{F} &= \begin{pmatrix} 1 & 0 \\ \psi_X & 1 \end{pmatrix}, \\ \mathbb{B} &= \begin{pmatrix} 1 & \psi_X \\ \psi_X & 1 + \psi_X^2 \end{pmatrix}, \\ \mathbf{v} &= \begin{pmatrix} 0 \\ \psi_t \end{pmatrix}, \\ E_{\mathbf{m}} &= \mathbf{v}, \\ E_{\rho} &= -\frac{1}{2} \mathbf{v}^2 + \frac{\mu}{2} (\text{tr}(\mathbb{B}) - 2 - \ln(\det(\mathbb{B}))), \\ E_s &= 0, \\ E_{B_{11}} &= \rho \frac{\mu}{2} (1 - B_{22}) = -\rho \frac{\mu}{2} \psi_X^2, \\ E_{B_{22}} &= \rho \frac{\mu}{2} (1 - B_{22}) = 0, \\ E_{B_{12}} &= \rho \frac{\mu}{2} B_{21} = \rho \frac{\mu}{2} \psi_X, \\ E_{B_{21}} &= \rho \frac{\mu}{2} B_{12} = \rho \frac{\mu}{2} \psi_X. \end{aligned}$$

Furthermore, we find that  $\rho, s = \text{const.}$  fulfil the equations. Then, plugging the above calculated values into equation (1.8) and performing a few simplifications, we get

$$\begin{pmatrix} 0 & \partial_t \psi_X \\ \partial_t \psi_X & 2\psi_X \partial_t \psi_X \end{pmatrix} = \begin{pmatrix} 0 & \partial_x \psi_t \\ \partial_x \psi_t & 2\psi_X \partial_x \psi_t \end{pmatrix},$$

which holds since  $x = X$ . Finally, performing analogical computations for  $m_1$  and  $m_2$  gives:

$$\begin{aligned} 0 &= \partial_t m_1 = \rho \partial_x \left( \frac{\mu}{2} (\text{tr}(\mathbb{B}) - 2 - \ln(\det(\mathbb{B}))) \right) \\ &\quad - \partial_x B_{jk} E_{B_{jk}} + \partial_x (B_{1k} (E_{B_{1k}} + E_{B_{k1}})) \\ &= \rho \mu \psi_X \partial_x \psi_X - \rho \mu \psi_X \partial_x \psi_X + \partial_x (-\rho \mu \psi_X^2) + \partial_x (\psi_X (\rho \mu \psi_X)) \\ &= 0 \end{aligned}$$

and

$$\begin{aligned}
\rho\psi_{tt} &= \partial_t m_2 = \partial_x(B_{1k}(E_{B_{2k}} + E_{B_{k2}})) \\
&= \partial_x(\rho\mu\psi_X) + \partial_x(\psi_X\rho\mu(1-1)) \\
&= \rho\mu\partial_x\psi_X,
\end{aligned}$$

which yields after division by  $\rho$

$$\psi_{tt} = \mu\psi_{xx}.$$

Thus the problem is reformulated to the one-dimensional wave equation, that can be solved by the Fourier method or d'Alembert formula.

### 3.3 Vertical Vibrations under the SHTC Model

Let us now assume the very same problem in the same geometry, only under the elastic SHTC model without the reduction to two dimensions. That is, we take

$$\begin{pmatrix} x \\ y \\ z \end{pmatrix} = \begin{pmatrix} X \\ Y + \psi(X, t) \\ Z \end{pmatrix},$$

use equations (1.11) – (1.14) and the energy

$$\int \frac{1}{2\rho} \mathbf{m}^2 + \rho \frac{c_s^2}{4} \|\text{dev}(\mathbb{G})\|_F + \varepsilon_{\text{micro}}(\rho, s) \, \mathbf{d}\mathbf{x}.$$

We also assume  $\rho_0, s_0 = \text{const.}$  Then, similarly as above,  $\rho, s = \text{const.}$  and because terms containing  $\varepsilon_{\text{micro}}$  are present only under some space derivatives, we may drop  $\varepsilon_{\text{micro}}$  from our computations.

Similarly as above, we get

$$\begin{aligned}
\mathbb{F} &= \begin{pmatrix} 1 & 0 & 0 \\ \psi_X & 1 & 0 \\ 0 & 0 & 1 \end{pmatrix}, \\
\mathbb{A} &= \begin{pmatrix} 1 & 0 & 0 \\ -\psi_X & 1 & 0 \\ 0 & 0 & 1 \end{pmatrix}, \\
\mathbf{v} &= \begin{pmatrix} 0 \\ \psi_t \\ 0 \end{pmatrix}, \\
E_{\mathbf{m}} &= \mathbf{v} \\
E_{\rho} &= -\frac{1}{2} \mathbf{v}^2 + \frac{c_s^2}{4} \|\text{dev}(\mathbb{G})\|_F, \\
E_s &= 0.
\end{aligned}$$

Next, we compute  $E_{\mathbb{A}}$  as

$$\begin{aligned}
\frac{\delta E}{\delta A_{ij}} &= \frac{\delta E}{\delta G_{ab}} \frac{\partial G_{ab}}{\partial A_{ij}} \\
&= \rho \frac{c_s^2}{4} \left( -\frac{2}{3} \text{tr}(\mathbb{G}) \delta_{ab} + 2G_{ab} \right) (A_{ib} \delta_{aj} + A_{ia} \delta_{bj}) \\
&= \rho c_s^2 \left( -\frac{1}{3} \text{tr}(\mathbb{G}) A_{ij} + G_{ja} A_{ia} \right),
\end{aligned} \tag{3.5}$$

thus, using

$$\text{dev}(\mathbb{G}) = \begin{pmatrix} \frac{2}{3} \psi_X^2 & -\psi_X & 0 \\ -\psi_X & -\frac{1}{3} \psi_X^2 & 0 \\ 0 & 0 & -\frac{1}{3} \psi_X^2 \end{pmatrix},$$

we obtain

$$\begin{aligned}
E_{A_{11}} &= \rho c_s^2 \frac{2}{3} \psi_X^2 \\
E_{A_{21}} &= \rho c_s^2 \left( -\psi_X - \frac{2}{3} \psi_X^3 \right) \\
E_{A_{31}} &= 0.
\end{aligned}$$

Now, by once again plugging the results above into equation (1.14), we get

$$\begin{pmatrix} 0 & 0 & 0 \\ -\partial_t \psi_X & 0 & 0 \\ 0 & 0 & 0 \end{pmatrix} = \begin{pmatrix} 0 & 0 & 0 \\ -\partial_x \psi_t & 0 & 0 \\ 0 & 0 & 0 \end{pmatrix},$$

which holds.

Finally, we focus on the equations for momenta:

$$\begin{aligned}
0 = \partial_t m_1 &= -\rho \partial_x \left( \frac{c_s^2}{4} \|\text{dev}(\mathbb{G})\|_F \right) - A_{j1} \partial_x E_{A_{j1}} \\
&= -\rho \left( c_s^2 \psi_X \partial_x \psi_X + c_s^2 \frac{2}{3} \psi_X^3 \partial_x \psi_X - \frac{4}{3} c_s^2 \psi_X \partial_x \psi_X \right) \\
&\quad - \rho \left( +2c_s^2 \psi_X^3 \partial_x \psi_X + c_s^2 \psi_X \partial_x \psi_X \right) \\
&= \rho c_s^2 \frac{4}{3} \psi_{xx} (\psi_x^3 - \psi_x), \\
\rho \psi_{tt} = \partial_t m_2 &= -A_{j2} \partial_x E_{A_{j1}} \\
&= \rho c_s^2 \psi_{xx} (\psi_x^2 + 1), \\
0 = \partial_t m_3 &= -A_{j3} \partial_x E_{A_{j1}} = 0.
\end{aligned}$$

The last equation holds identically. However, if the first one holds, it means  $0 = \psi_{xx} (\psi_x^3 - \psi_x)$ , which holds only if  $\psi_{xx} = 0$ ,  $\psi_x = 0$ , or  $\psi_x = \pm 1$ . This implies  $\psi_{xx} = 0$ . To show that, let  $x_1$  be such that  $\psi_{xx}(x_1) \neq 0$ . Then  $\psi_x(x_1) \in \{-1, 0, 1\}$ . However, then at some  $x_2$  close to  $x_1$  it holds  $\psi_{xx}(x_2) \neq 0$  (from continuity of  $\psi_{xx}$ ) and  $\psi_x(x_2) \notin \{-1, 0, 1\}$  (since  $\psi_{xx}(x_2) \neq 0$ ).

However, the equation for  $m_2$  then implies that  $\psi_{tt} = 0$ . Thus the only possible solution of this problem is linear in both  $x$  and  $t$ . This surely is an

analytic solution, but cannot capture wave-like behaviour of an elastic solid that we expect. We thus infer that it is necessary to permit the particles to move in the direction of the  $x$ -axis for a more complex motion to exist.

We may further linearise the problem, which makes all terms zero, with the exception of

$$\rho\psi_{tt} = \rho c_s^2 \psi_{xx}.$$

Thus, dividing by  $\rho$ , we get the wave equation

$$\psi_{tt} = c_s^2 \psi_{xx}$$

once again.

### 3.4 Numerical Solution to the Vibrations under SHTC Model

In this section, we numerically solve the elastic SHTC model for a solid<sup>2</sup> under suitable boundary conditions and initial conditions and compare it to the exact solution of the linearised problem. Let us take the initial conditions as

$$\begin{aligned}\psi(x, 0) &= \psi_0(x), \\ v_2(x, 0) = \psi_t(x, 0) &= 0\end{aligned}$$

where  $\psi_0(x)$  is a periodic function with period of unit length. Then the exact solution is given according to d'Alembert by

$$\psi(x, t) = \frac{1}{2} (\psi_0(x + c_s t) + \psi_0(x - c_s t))$$

and thus

$$\psi_t(x, t) = \frac{c_s}{2} (\psi_0'(x + c_s t) - \psi_0'(x - c_s t)).$$

Moreover, from periodicity of the problem, we get  $\psi(x, t) = \psi(x, t + P)$  for every  $t$  and  $P = \frac{1}{c_s} = \frac{1}{2141}$ . Furthermore, periodicity enables us to model this problem on  $x \in (0, 1)$  with space discretization over the  $x$ -axis and periodic boundary conditions.

Let us take

$$(y =) \psi_0(x) = \begin{cases} \frac{1}{50}x & x < 0.25 \\ \frac{-1}{50}x + \frac{1}{100} & 0.25 \leq x \leq 0.75 \\ \frac{1}{50}x - \frac{1}{50} & x > 0.75 \end{cases}.$$

Figure 3.1 shows the initial configuration.

In the numerical, which is described in appendix A.4, we prescribe the initial conditions by taking  $\rho(x, 0) = \rho_0$ ,  $\mathbf{v}(x, 0) = 0$  and

$$\mathbb{A}(x, 0) = \begin{pmatrix} 1 & 0 & 0 \\ -1/50 & 1 & 0 \\ 0 & 0 & 1 \end{pmatrix}$$

---

<sup>2</sup>See tables A.1, A.2, and A.3 in appendix A.5 for material parameters chosen.

for  $x \in (0.25, 0.75)$  and

$$\mathbb{A}(x, 0) = \begin{pmatrix} 1 & 0 & 0 \\ 1/50 & 1 & 0 \\ 0 & 0 & 1 \end{pmatrix}$$

else.

Having this, we directly compute  $\rho, \mathbf{m}, \mathbb{A}, \varepsilon$ . From these  $\mathbf{v}$  may be obtained as  $\frac{m}{\rho}$ , while  $(y =) \psi$  by integrating  $\mathbb{A}^{-1} = \mathbb{F}$  over  $X$ . Figures 3.2 and 3.3 show very similar behaviour of both the  $y$ -velocities and positions of the numerical and exact solution at time  $t = 0.00005$ . Figure 3.4 shows the  $x$ -velocities at  $t = 0.00005$ , which are clearly non-zero, though considerably smaller than  $y$ -velocities. This result has been expected in the previous section. Finally figures 3.5 and 3.6 compare  $y$ -velocities and positions of the numerical solutions at times  $t = 0.00005$ ,  $t = 0.00005 + P$  and  $t = 0.00005 + 2P$ . One may see that they slightly mollify over the time (because of numerical error). They, however, have equal amplitude occurring at the same point.

The same problem can be also solved with more smooth initial conditions, for example

$$(y =) \psi_0(x) = \frac{1}{100\pi} \sin(2\pi x) \quad (3.6)$$

Figures 3.7 and 3.8 show very good results for this scheme, both in accuracy at  $t = 0.00005$  and periodicity.

Altogether, we conclude that the numerical solution gives slightly different results<sup>3</sup> – mostly because of the numerical error – but is very similar to the analytic solution to the linearised problem. One may see, however, a fundamental difference between the two models in the fact that the numerical solutions exhibits non-zero velocities in the  $x$ -direction.

### 3.5 Elastoplastic Vibrations

We may further numerically model the very same problem, however, adding the dissipation. This models the vibrations in an elastoplastic solid (instead of an elastic one). The figures 3.9 and 3.10 compare  $y$ -velocities of the dissipating solutions at times  $t = 0.00005$ ,  $t = 0.00005 + P$  and  $t = 0.00005 + 2P$  for the non-smooth and smooth data, respectively. It is clearly visible that the motion is very similar to that of an elastic material, but the speeds are decreasing. This slowing-down behaviour is exactly what would one expect from model with dissipation. Furthermore, the energy lost due to dissipation is transformed to heat, as is obvious from temperature increase in figure 3.11. Note that the scheme neglects heat fluxes, causing high temperature differences along the body.

---

<sup>3</sup>The difference is unsurprisingly greater for the non-smooth data. However, the approximation is still very good.

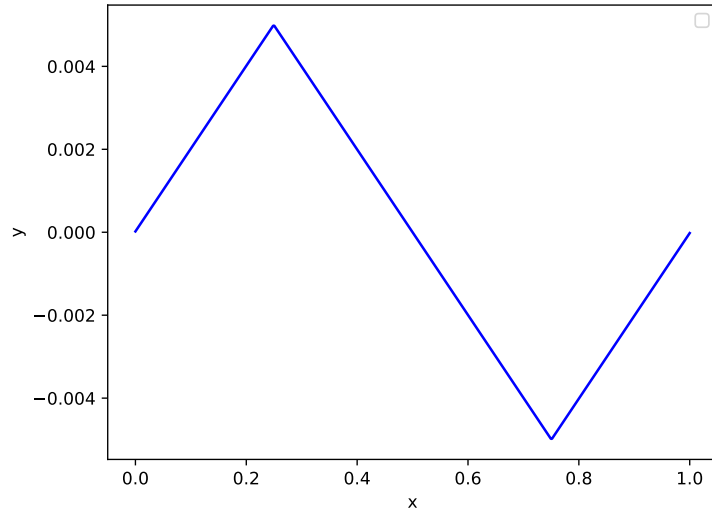


Figure 3.1: Vertical vibrations in elastic solid: One initial  $y$ -deformation of the problem.

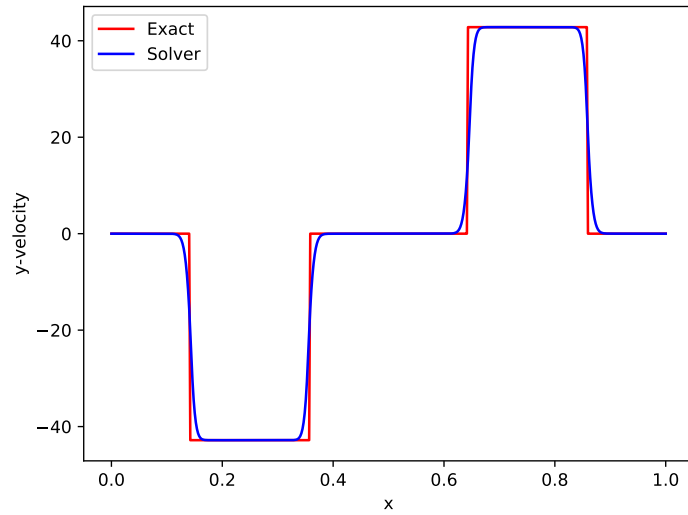


Figure 3.2: Vertical vibrations in elastic solid: Numerical solution to the full problem with initial deformation in one dimension under the SHTC model (blue) and exact solution to the linearised problem – wave equation – (red);  $y$ -velocities at time  $t = 0.00005$  with mesh of 500 cells; piece-wise linear IC, periodic BC. The two solutions nearly match.

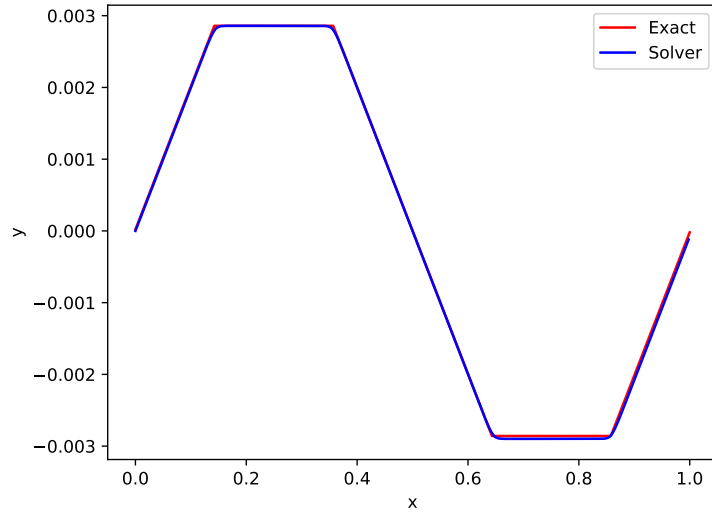


Figure 3.3: Vertical vibrations in elastic solid: Numerical solution to the full problem with initial deformation in one dimension under the SHTC model (blue) and exact solution to the linearised problem – wave equation – (red);  $y$ -positions at time  $t = 0.00005$  with mesh of 500 cells; piece-wise linear IC, periodic BC. The two solutions nearly match.

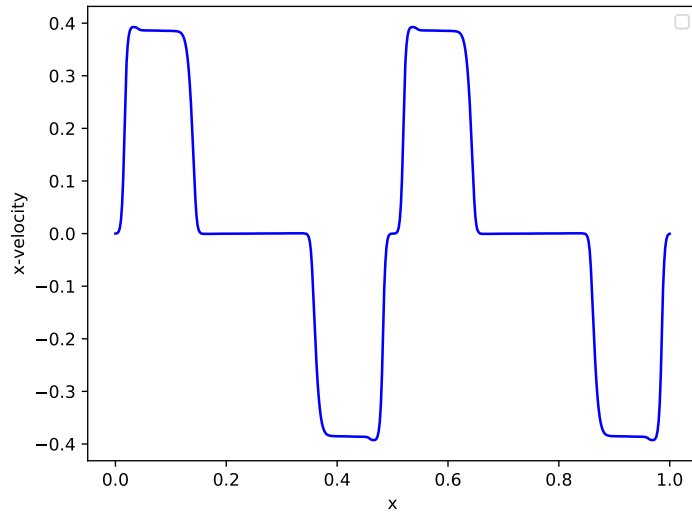


Figure 3.4: Vertical vibrations in elastic solid: Numerical solution to the full problem with initial deformation in one dimension under the SHTC model; non-zero  $x$ -velocities at time  $t = 0.00005$  with mesh of 500 cells. A result not observed in the linearised problem or under the neo-Hookean model; piece-wise linear IC, periodic BC.

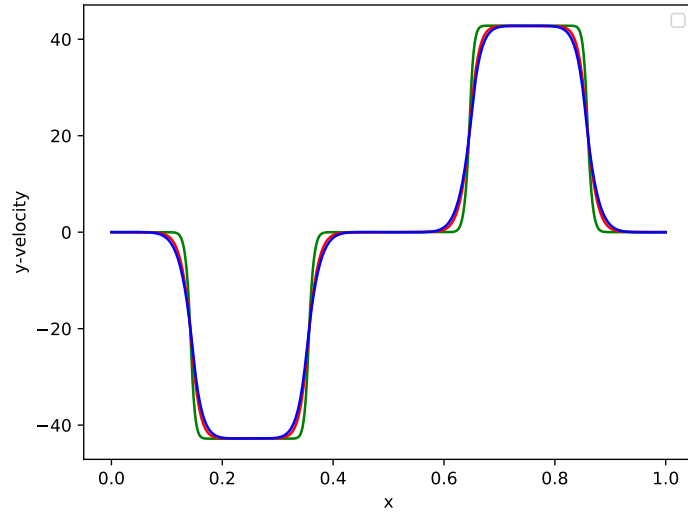


Figure 3.5: Vertical vibrations in elastic solid: Numerical solution to the full problem with initial deformation in one dimension under the SHTC model at time  $t = 0.00005$  (green),  $t = 0.00005 + P$  (red) and  $t = 0.00005 + 2P$  (blue), where  $P = \frac{1}{2141}$  is the period of the linearised elastic problem;  $y$ -velocities with mesh of 500 cells; piece-wise linear IC, periodic BC. We can see a nearly periodic behaviour of the numerical solution.

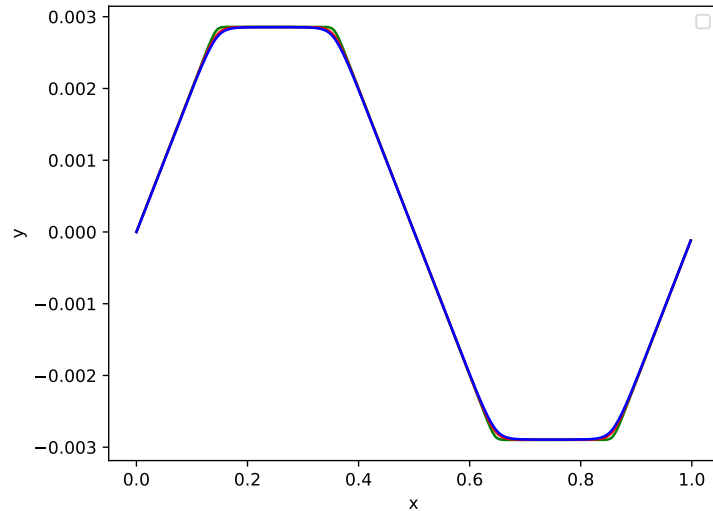


Figure 3.6: Vertical vibrations in elastic solid: Numerical solution to the full problem with initial deformation in one dimension under the SHTC model at time  $t = 0.00005$  (green),  $t = 0.00005 + P$  (red) and  $t = 0.00005 + 2P$  (blue), where  $P = \frac{1}{2141}$  is the period of the linearised elastic problem;  $y$ -positions with mesh of 500 cells; piece-wise linear IC, periodic BC. We can see a nearly periodic behaviour of the numerical solution.

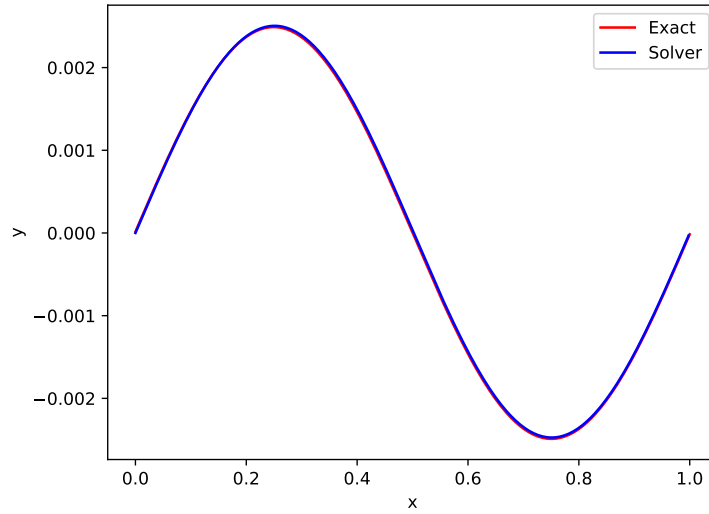


Figure 3.7: Vertical vibrations in elastic solid: Numerical solution to the full problem with initial deformation in one dimension under the SHTC model (blue) and exact solution to the linearised problem – wave equation – (red);  $y$ -positions at time  $t = 0.00005$  with mesh of 500 cells; sinusoid IC, periodic BC. The two solutions nearly match.

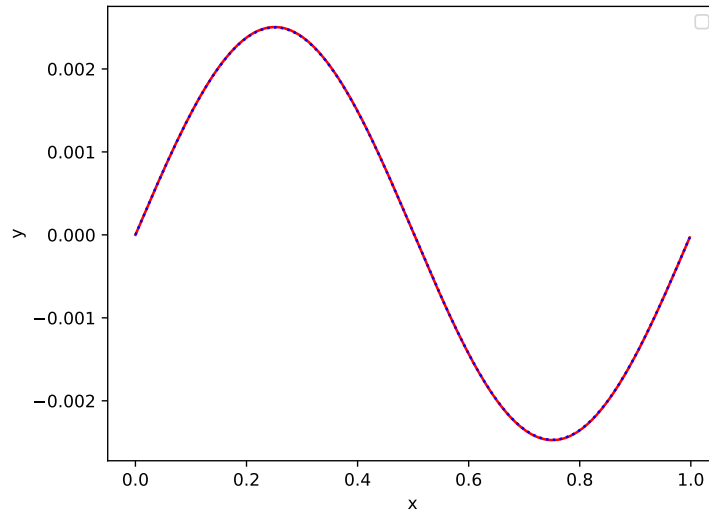


Figure 3.8: Vertical vibrations in elastic solid: Numerical solution to the full problem with initial deformation in one dimension under the SHTC model at time  $t = 0.00005$  (red solid line) and  $t = 0.00005 + \frac{1}{2141}$  (blue dotted line);  $y$ -positions with mesh of 500 cells; sinusoid IC, periodic BC. We can see a nearly periodic behaviour of the numerical solution.

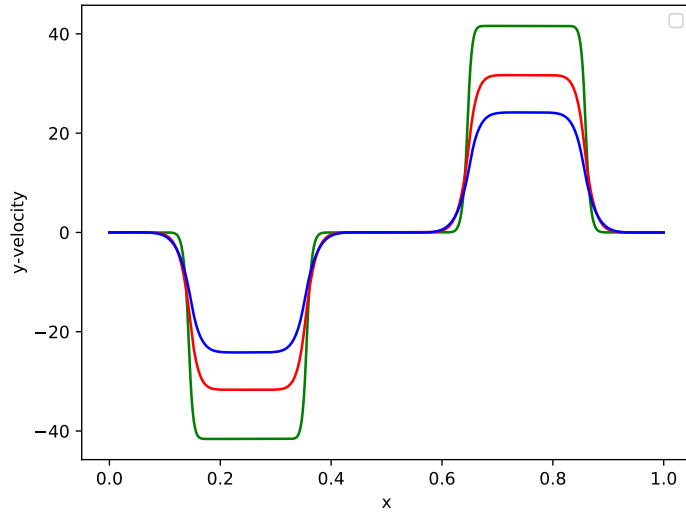


Figure 3.9: Vertical vibrations in elastoplastic solid: Numerical solution to the problem with initial deformation in one dimension under the SHTC model with dissipation at the time  $t = 0.00005$  (green),  $t = 0.00005 + P$  (red) and  $t = 0.00005 + 2P$  (blue), where  $P = \frac{1}{2141}$  is the period of the linearised elastic problem;  $y$ -velocities with mesh of 500 cells; piece-wise linear IC, periodic BC. The dissipation causes decrease in velocities.

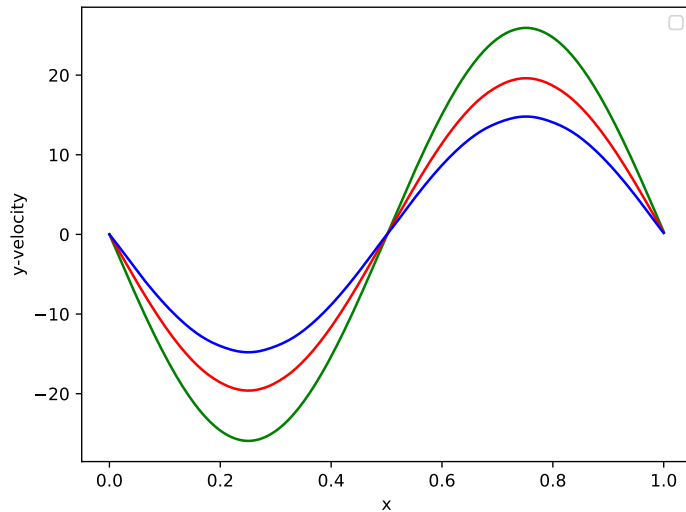


Figure 3.10: Vertical vibrations in elastoplastic solid: Numerical solution to the problem with initial deformation in one dimension under the SHTC model with dissipation at the time  $t = 0.00005$  (green),  $t = 0.00005 + P$  (red) and  $t = 0.00005 + 2P$  (blue), where  $P = \frac{1}{2141}$  is the period of the linearised elastic problem;  $y$ -velocities with mesh of 500 cells; sinusoid IC, periodic BC. The dissipation causes decrease in velocities. The energy lost in speed is compensated by temperature growth.

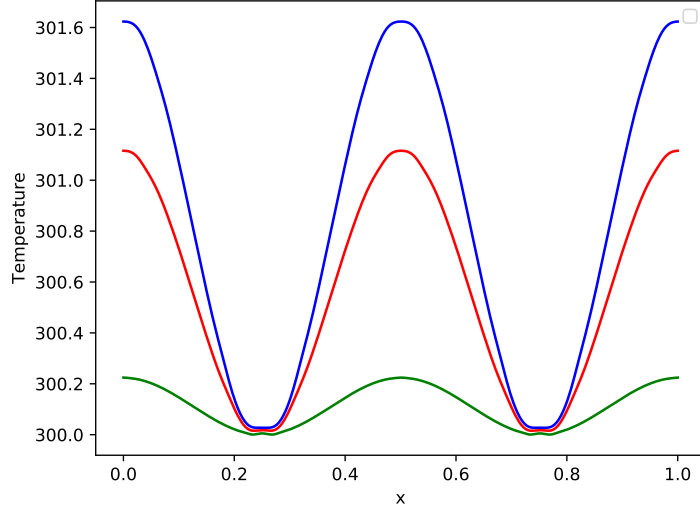


Figure 3.11: Vertical vibrations in elastoplastic solid: Numerical solution to the problem with initial deformation in one dimension under the SHTC model with dissipation at the time  $t = 0.00005$  (green),  $t = 0.00005 + P$  (red) and  $t = 0.00005 + 2P$  (blue), where  $P = \frac{1}{2141}$  is the period of the linearised elastic problem; temperature with mesh of 500 cells; sinusoid IC, periodic BC.

### 3.6 Simple Shear

Let us now assume a special case of the motion presented in section 3.3. That is, we take the analytic linear solution

$$\psi(x, t) = 100xt,$$

that is, a specific simple shear. We further restrict the domain to  $x \in [0, 1]$  and specify the BC as  $v_2(0, t) = 0$ ,  $v_2(1, t) = 100$  and the initial conditions as  $\mathbb{A}(x, 0) = \mathbb{I}$ ,  $\rho(x, 0) = \rho_0$  and  $v(x, 0) = 100x$ .<sup>4</sup> Then  $\psi$  is the analytic solution to this Dirichlet problem. Here,  $\psi_x$  measures the shear rate.<sup>5</sup> Let us find out the shear stress  $T_{yx} = \sigma_{yx}$ . Recalling (3.5) and (1.15), one has

$$\begin{aligned} \sigma_{il} &= -\rho c_s^2 A_{Li} \left( -\frac{1}{3} \text{tr}(\mathbb{G}) A_{Ll} + G_{la} A_{La} \right) \\ &= -\rho c_s^2 \left( G_{la} G_{ia} - \frac{1}{3} \text{tr}(\mathbb{G}) G_{li} \right), \end{aligned}$$

which implies

$$\sigma = -\rho c_s^2 \mathbb{G} \text{dev}(\mathbb{G}).$$

Note that this relation holds universally for the SHTC model. In the assumed

<sup>4</sup>In other words, the BC and IC are  $\psi(0, t) = 0$ ,  $\psi(1, t) = 100t$ ,  $\psi(x, 0) = 0$  and  $\psi_t(x, 0) = 100x$

<sup>5</sup>Which we define as  $F_{yx}$ , where  $\mathbb{F}$  is the deformation gradient.

geometry, straightforward computations lead to the relation:<sup>6</sup>

$$\sigma = -\rho c_s^2 \begin{pmatrix} \frac{5}{3}\psi_x^2 + \frac{2}{3}\psi_x^4 & -\psi_x - \frac{2}{3}\psi_x^3 & 0 \\ -\psi_x - \frac{2}{3}\psi_x^3 & \frac{2}{3}\psi_x^2 & 0 \\ 0 & 0 & -\frac{1}{3}\psi_x^2 \end{pmatrix}.$$

Finally,

$$T_{yx}(\psi_x) = \rho c_s^2 \left( \psi_x + \frac{2}{3}\psi_x^3 \right)$$

is the stress strain relation. We now compute it numerically for an elastic solid in a simulation with 100 cells, the BC and IC of which are specified above. First, we verify if the numerical solution is the expected simple shear. We plot velocities in  $x$  and  $y$  direction at five different times between  $t = 0$  and  $t = 0.01$ . As we see in figures 3.12 and 3.13, the  $y$ -velocities match expectations perfectly. The  $x$ -velocities are non-zero – perhaps because of minor inaccuracy at boundary conditions – although so small that we neglect them. The stress-strain relation is then measured at each time step.  $F_{yx}$  is reconstructed as  $A_{yx}^{-1}$  and  $T_{yx}$  is calculated numerically from the solution in the cell 50. Figure 3.14 shows the resulting shear rate – shear stress relation approximately matching the expected super linear growth.

The same can be numerically performed with dissipation. Figures 3.15 and 3.16 verify that the motion is also nearly simple shear. Thus, the  $x$ -velocities are neglected and shear rate is calculated as  $100t$ . Note, that we do not use the solved  $\mathbb{A}$ , since it is degenerated (see the following paragraph). The resulting shear rate – shear stress relationship is, however, sub-linear, even perhaps bounded, as shown in figure 3.17.

Moreover, we compute the Frobenius norm of  $\text{curl}(\mathbb{A})$ . The derivatives in the curl are estimated by central difference<sup>7</sup>. Figure 3.18 shows this is equal to 0. Thus we integrate  $\mathbb{A}^{-1}$ . In the elastic case, this procedure creates the actual configuration. The line segment  $y = 0$  from the reference configuration is mapped approximately to the line  $y = x$  in the actual configuration at time  $t = 0.01$ . The comparison of this true result and the integral of  $\mathbb{A}^{-1}$  is presented in figure 3.19. It is obvious that  $\mathbb{A}$  has no longer the meaning of the inverse of the deformation gradient, even though its curl is zero.<sup>8</sup> This result is not surprising: The evolution equation for distortion matrix is different in elastic and elastoplastic case; and since  $\mathbb{A}$  is the inverse of deformation gradient in the elastic solid, it can hardly be the same in the elastoplastic solid.

The author of this thesis humbly suggest a possible interpretation of  $\mathbb{A}$  in the case of non-zero dissipation and zero  $\text{curl}(\mathbb{A})$ :  $\mathbb{A}$  is still unambiguously integrable, but its integral does not represent a connection between actual and reference configurations. This is caused by the dissipation. Therefore, one may think that  $\mathbb{A}$  stores the information only about the elastic part of the motion, thus forming the connection between the actual and natural configuration. However, this is only a personal opinion without any ambitions to be precise.

<sup>6</sup>This result holds for any  $\psi$  solving the problem from section 3.3.

<sup>7</sup>Forward and backward difference are applied upon the boundary.

<sup>8</sup>The integral is computed by rectangle rule, which is a very basic tool. However, such a big difference cannot be explained by that.

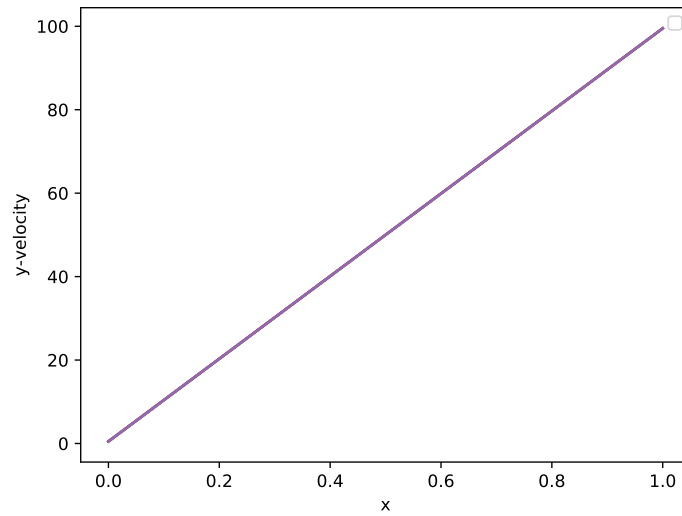


Figure 3.12: Simple shear in elastic solid:  $y$ -velocities are plotted at five different times. Their linearity in all cases verifies that the simulated motion is close to a simple shear.

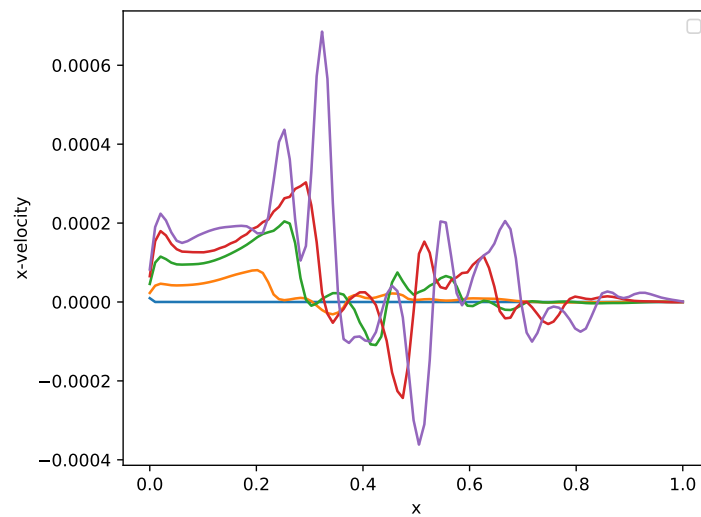


Figure 3.13: Simple shear in elastic solid:  $x$ -velocities are plotted at five different times. Even though they are not exactly zero, they are very low. This verifies that the simulated motion is close to a simple shear.

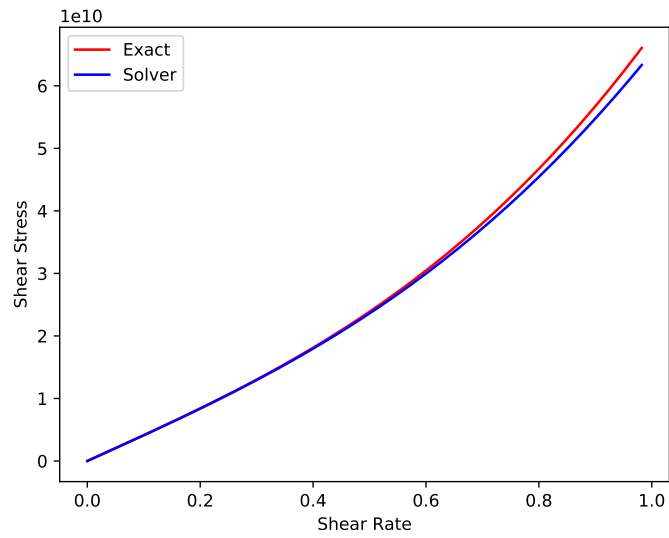


Figure 3.14: Simple shear in elastic solid: Comparison of the measured relation between shear rate (measured as  $A_{yx}^{-1}$ ) and computed shear stress and the analytic one found in section 3.6.

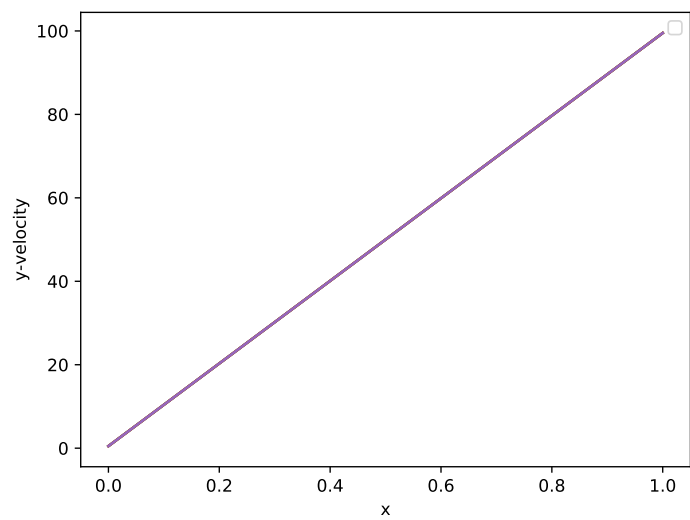


Figure 3.15: Simple shear in elastoplastic solid:  $y$ -velocities are plotted at five different times. Their linearity in all cases verifies that the simulated motion is close to a simple shear.

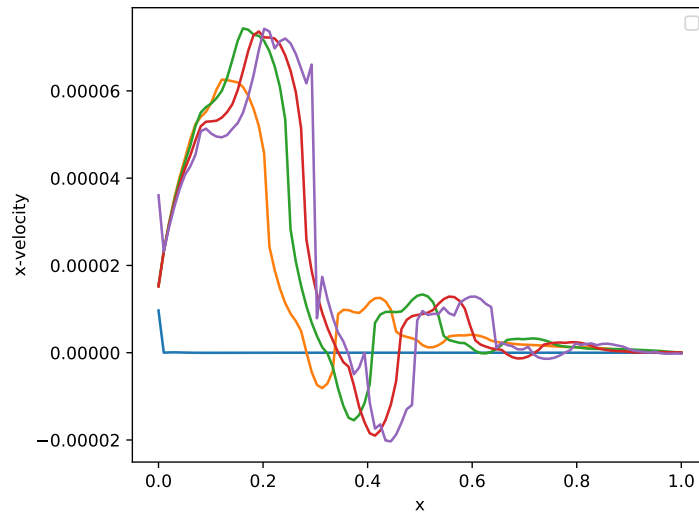


Figure 3.16: Simple shear in elastoplastic solid:  $x$ -velocities are plotted at five different times. Even though they are not exactly zero, they are very low. This verifies that the simulated motion is close to a simple shear.

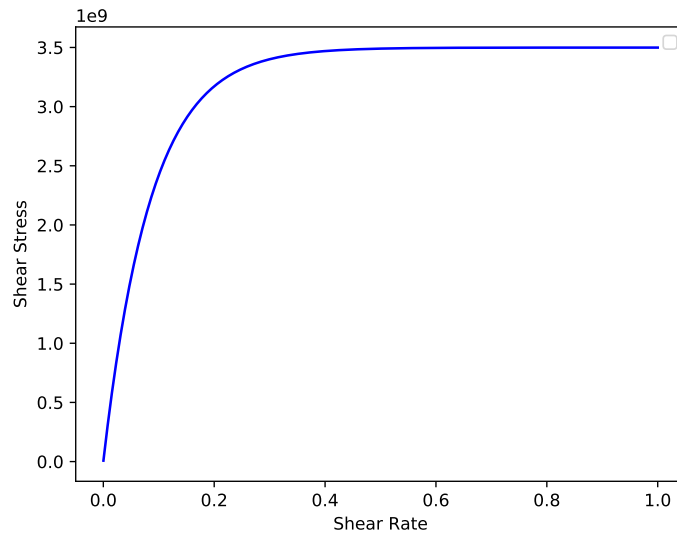


Figure 3.17: Simple shear in elastoplastic solid: The relation between shear rate (measured as  $100t$ ) and computed shear stress. Note, that it is growing sub linearly and seems to be bounded, unlike the one in elastic solid.

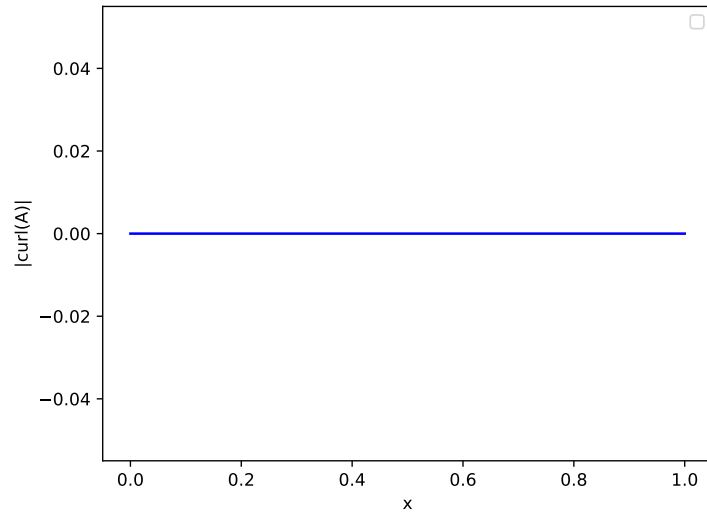


Figure 3.18: Simple shear in elastoplastic solid: The Frobenius of the Burgers tensor, which was calculated from the values of  $\mathbb{A}$  by central differences. Since it is zero, integration of  $\mathbb{A}$  does not depend on the integration path.

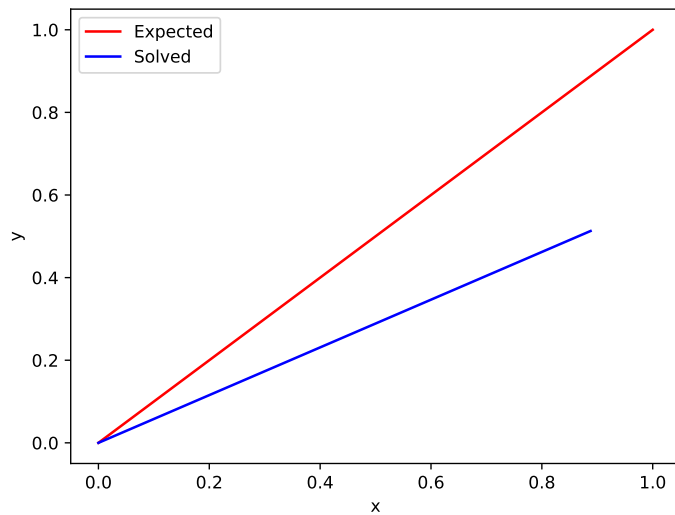


Figure 3.19: Simple shear in elastoplastic solid: Comparison of the real – or expected – deformation and the deformation reconstructed by integrating  $\mathbb{A}^{-1}$  over the reference configuration. Even though the  $\text{curl}(\mathbb{A}) = 0$ . This clearly demonstrates that the connection between reference and actual configuration is lost, considering a motion with dissipation.

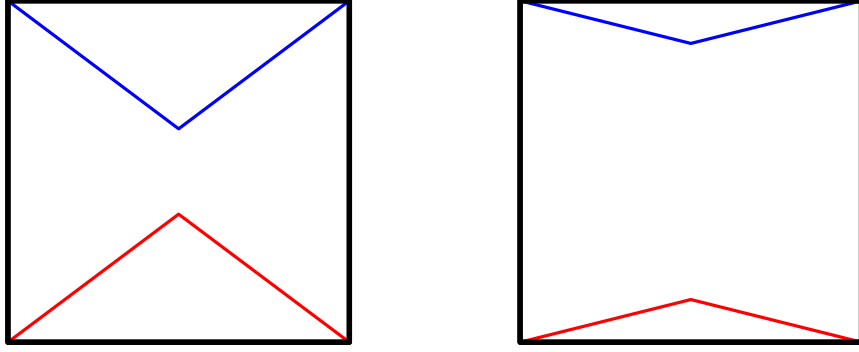


Figure 3.20: The reference (left) and initial configuration. The blue and red lines are mapped to themselves by moving each particle only in the vertical direction; not to scale.

### 3.7 Elastoplastic Solid in Two Dimensions

In the last example for a solid, we model a two-dimensional elastoplastic body on a unit square with the initial configuration given by figure 3.20, i.e., by moving each particle only in the vertical (or  $y$ -) direction, we reduce the height of the shown triangles from 0.21 to 0.20. This compression and extension is linear in  $y$  on each of the triangles and the space between them. Periodic boundary conditions are applied. We study the distribution of density and the Frobenius norm of the Burgers tensor, that is,  $\text{curl}(\mathbb{A})$ . Figure 3.21 shows the initial mass density over a  $1000 \times 1000$  mesh. Figures 3.22 and 3.23 show the mass density and the norm of the Burgers tensor at time  $t = 0.00001$  over the mesh  $200 \times 200$ . The Burgers tensor has highest norm around the jump in density. Note, however, that the values are very low and may be caused by a numerical error only.

### 3.8 Couette Flow

In this section, we demonstrate that the SHTC equations can describe fluids as well.<sup>9</sup> Our aim is to model the planar Couette flow, i.e., a laminar flow between two parallel planes with no-slip boundary conditions. One of them is motionless, the other moving at a constant rate. The well-known stationary solution is a linear velocity profile.

In this case, we set the BC as  $v_2|_{x=0} = 0$  and  $v_2|_{x=0.25} = 0.25$ . Thus, the solution is  $v_2(x) = x$ . Moreover, with zero velocity as initial condition, White [2006]<sup>10</sup> has derived that the velocity profile at time  $t$  is given by:

$$\frac{v}{V} = \left(1 - \frac{x}{h}\right) - \frac{2}{\pi} \sum_{n=1}^{\infty} \frac{1}{n} \text{ext} \left( -n^2 \pi^2 \frac{\nu t}{h^2} \right) \sin \left( \frac{n\pi x}{h} \right),$$

where  $\nu$  is the kinematic viscosity,  $h$  the distance between the two planes and  $V$  the speed of the moving plane. We thus model this situation with a known result. We take  $\mu = 10^{-2}$ ,  $v_0 = 0$ ,  $\mathbb{A}_0 = \mathbb{I}$  and  $p_0 = \frac{1}{\gamma}$ . The resulting convergence

<sup>9</sup>See tables A.1, A.2, and A.3 in appendix A.5 for material parameters used.

<sup>10</sup>See section 3-5.2.

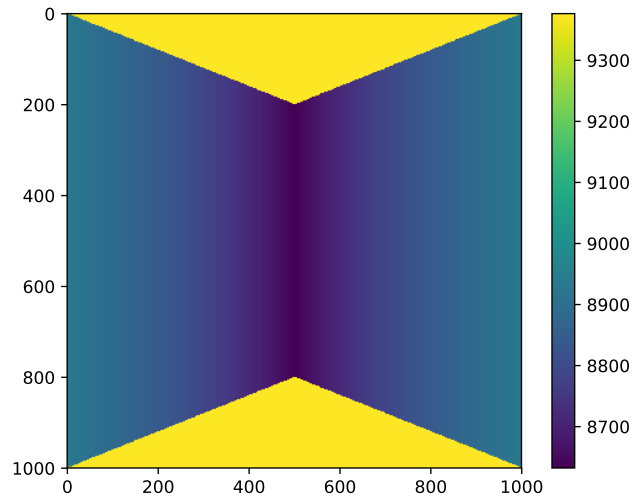


Figure 3.21: Elastoplastic solid in two dimensions; density at time  $t = 0$  with  $1000 \times 1000$  cells. The axes do not describe the actual position, but the cell coordinates.

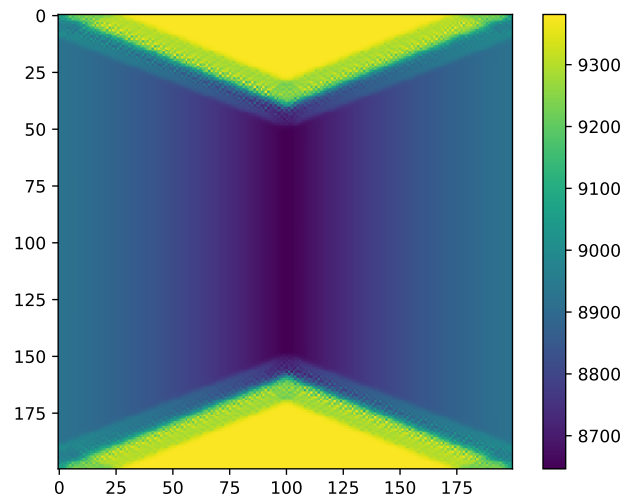


Figure 3.22: Elastoplastic solid in two dimensions; density at time  $t = 0.00001$  with  $200 \times 200$  cells. One can see the expected propagation of the density from the compressed to the extended part of the body. The axes do not describe the actual position, but the cell coordinates.

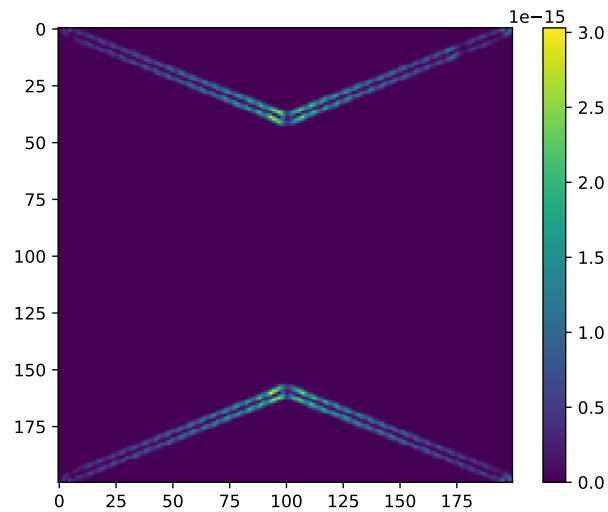


Figure 3.23: Elastoplastic solid in two dimensions; Frobenius norm of the Burgers tensor at time  $t = 0.00001$  with  $200 \times 200$  cells. One can see it is non-zero around the jump in density. The axes do not describe the actual position, but the cell coordinates.

to the linear velocity profile is shown in figure 3.24. It matches the exact solution presented by White [2006] very well.

If we start with initial velocity closer to the stationary solution, we expect faster convergence. This is demonstrated by figure 3.25, which shows very fast convergence with  $v_0 = 0.125 + 0.125 \cos(\pi + 4\pi x)$ . If we decrease the viscosity  $\mu$  by one order to  $\mu = 10^{-3}$ , the speed of convergence is dramatically slowed-down, see figure 3.26.

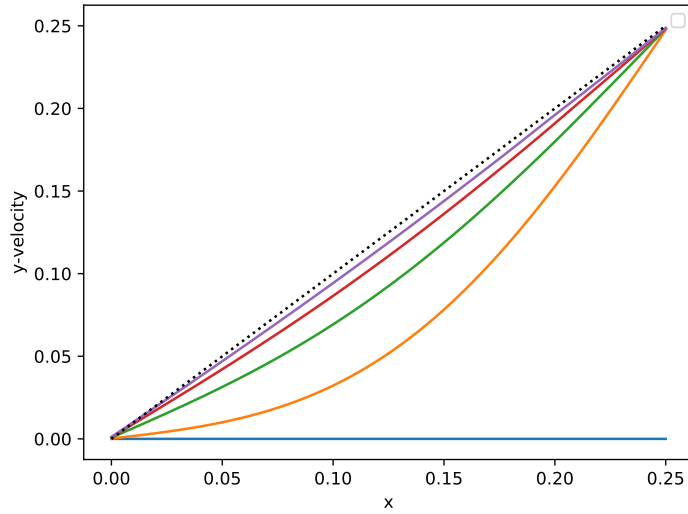


Figure 3.24: Couette flow between two planes at  $x = 0$  and  $x = 0.25$ . The velocity at  $t = 0$  is zero. Five velocity profiles approximately uniformly dividing the time interval  $t \in [0, 2]$  (coloured lines) are compared to the steady state linear profile (dotted line). The convergence matches the results of White [2006]. The viscosity is  $\mu = 10^{-2}$ .

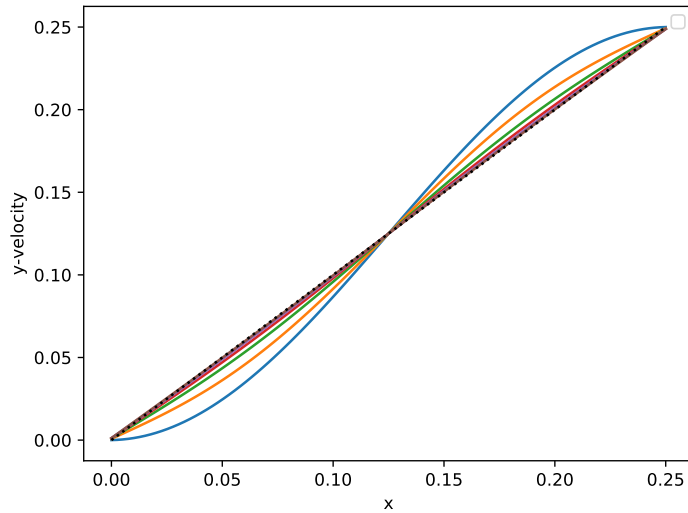


Figure 3.25: Couette flow between two planes at  $x = 0$  and  $x = 0.25$ . The velocity at  $t = 0$  is sinusoid (blue line). Five velocity profiles approximately uniformly dividing the time interval  $t \in [0, 0.5]$  (coloured lines) are compared to the steady state linear profile (dotted line). The viscosity is set to  $\mu = 10^{-2}$ . The speed of convergence is significantly higher than in the case  $\mu = 10^{-3}$ .

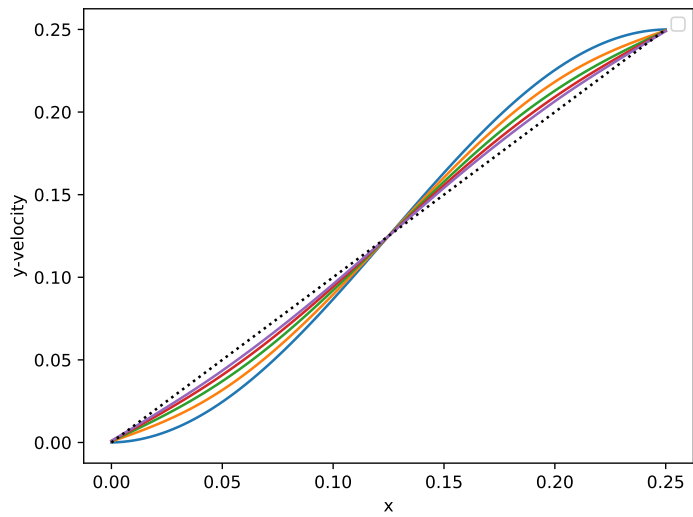


Figure 3.26: Couette flow between two planes at  $x = 0$  and  $x = 0.25$ . The velocity at  $t = 0$  is sinusoid (blue line). Five velocity profiles approximately uniformly dividing the time interval  $t \in [0, 2]$  (coloured lines) are compared to the steady state linear profile (dotted line). The viscosity is set to  $\mu = 10^{-3}$ . The speed of convergence is significantly lower than in the case  $\mu = 10^{-2}$ .

# Conclusion

In the first part of this text, we have described an elegant, but not very well known, way to obtain governing equations for a continuous body. It was shown that the compressible elastic neo-Hookean solid can be described by this formalism. Next, two models (SHTC and the “classical” neo-Hookean) were presented and compared on an example of vertical vibrations in an elastic solid. The neo-Hookean model can be viewed – in this specific example – as a linearisation of the SHTC model. The non-linearised SHTC model exhibits an interesting property that it does not allow particles to move strictly up and down without moving in the  $x$ -direction, as long as trivial solutions are ignored.

Numerical solution of the full problem was then compared to the exact solution of the problem linearised to a wave equation. The two solutions are very similar, including their periodicity, but the numerical solutions undergoes a movement in the horizontal direction.

Next, the simple shear was studied. The numerical scheme can model it – up to a small mistake in the  $x$ -velocities. Moreover, the numerically measured relation of shear rate and shear stress for an elastic solid approximately matches the analytic one. On the other hand, the relation differs greatly from that of an elastoplastic solid. We have also illustrated the interesting fact that the distortion matrix ceases to be the inverse of the deformation gradient under elastoplastic deformations.

The properties of the deformation gradient was next further studied in a more complex, two-dimensional motion to show that the  $\text{curl}(\mathbb{A})$  can become non-zero in the elastoplastic solid.

Finally Couette flow of a fluid was numerically tested. The solutions converge to the analytic stationary solution and – in case of zero initial velocity – the form of convergence agrees with the analytic results.

Thus, we have summarized the derivation of the governing equations by the GENERIC framework and compared it to the standard results. We have also studied some interesting properties of the equations – both analytically and numerically.

# Bibliography

- R. Byron Bird, Robert C. Armstrong, and Ole Hassager. *Dynamics of Polymeric Liquids*. Wiley-Interscience, 1987.
- Walter Boscheri, Michael Dumbser, and Raphaël Loubère. On direct arbitrary-lagrangian-eulerian ader-weno finite volume schemes for the hpr model of non-linear hyperelasticity. *International journal for numerical methods in fluids*, 134, 02 2016. doi: 10.1016/j.compfluid.2016.05.004.
- M. Dumbser, I. Peshkov, E. Romenski, and O. Zanotti. High order ADER schemes for a unified first order hyperbolic formulation of continuum mechanics: Viscous heat-conducting fluids and elastic solids. *Journal of Computational Physics*, 314:824–862, 2016.
- M. Dumbser, I. Peshkov, E. Romenski, and O. Zanotti. High order ADER schemes for a unified first order hyperbolic formulation of Newtonian continuum mechanics coupled with electro-dynamics. *Journal of Computational Physics*, 348: 298–342, 2017.
- Michael Dumbser, Francesco Fambri, Maurizio Tavelli, Michael Bader, and Tobias Weinzierl. Efficient implementation of ADER discontinuous Galerkin schemes for a scalable hyperbolic PDE engine. *arXiv e-prints*, art. arXiv:1808.03788, Aug 2018.
- S. K. Godunov. An interesting class of quasi-linear systems. *Dokl. Akad. Nauk SSSR*, Jul 1961.
- Miroslav Grmela and Hans Christian Öttinger. Dynamics and thermodynamics of complex fluids. i. development of a general formalism. *Phys. Rev. E*, 56: 6620–6632, Dec 1997. doi: 10.1103/PhysRevE.56.6620. URL <https://link.aps.org/doi/10.1103/PhysRevE.56.6620>.
- M. E. Gurtin, E. Fried, and L. Anand. *The mechanics and thermodynamics of continua*. Cambridge University Press, 2010.
- H. Jackson. A fast numerical scheme for the Godunov-Peshkov-Romenski model of continuum mechanics. *Journal of Computational Physics*, 2017.
- H. Jackson. *A Unified Framework for Simulationg Impact-Induced Detonation of a Combustible Material in an Elasto-Plastic Confiner*. PhD thesis, University of Cambridge, 2018.
- L. D. Landau and E. M. Lifshitz. *Theory of Elasticity, Second Edition*. Course of Theoretical Physics, Vol. 7. Peggamon Press, 1970.
- R. Menikoff. Complete Mie-Gruneisen Equation of State. Technical report, Los Alamos National Laboratory, 2016.
- Josef Málek, K.R. Rajagopal, and Karel Tůma. On a variant of the Maxwell and Oldroyd-B models within the context of a thermodynamic basis. *International*

*Journal of Non-Linear Mechanics*, 76, 05 2015. doi: 10.1016/j.ijnonlinmec.2015.03.009.

Hans Christian Öttinger and Miroslav Grmela. Dynamics and thermodynamics of complex fluids. ii. illustrations of a general formalism. *Phys. Rev. E*, 56: 6633–6655, Dec 1997. doi: 10.1103/PhysRevE.56.6633. URL <https://link.aps.org/doi/10.1103/PhysRevE.56.6633>.

M. Pavelka, V. Klika, and M. Grmela. *Multiscale Thermo-Dynamics*. De Gruyten, 2018.

Michal Pavelka, Ilya Peshkov, and Vaclav Klika. On Hamiltonian continuum mechanics. *arXiv e-prints*, art. arXiv:1907.03396, Jul 2019.

Ilya Peshkov, Evgeniy Romenski, and Michael Dumbser. A unified hyperbolic formulation for viscous fluids and elastoplastic solids. *arXiv e-prints*, art. arXiv:1705.02151, May 2017.

Ilya Peshkov, Evgeniy Romenski, and Michael Dumbser. Continuum mechanics with torsion. *Continuum Mechanics and Thermodynamics*, page 40, Apr 2019. doi: 10.1007/s00161-019-00770-6.

L. I Sedov. *Introduction to the mechanics of a continuous medium*. Adiwes international series in the engineering sciences. Addison-Wesley Pub. Co, 1965.

V. A. Tiarev and E. F. Toro. ADER: Arbitrary High Order Godunov Approach. *Journal of Scientific Computing*, 2001.

M. Frank White. *Viscous Fluid Flow, Third Edition*. McGraw-Hill Series in Mechanical Engineering. McGraw-Hill, 2006.

# List of Figures

3.1	Vertical vibrations in elastic solid: One initial $y$ -deformation of the problem. . . . .	30
3.2	Vertical vibrations in elastic solid: Numerical solution to the full problem with initial deformation in one dimension under the SHTC model (blue) and exact solution to the linearised problem – wave equation – (red); $y$ -velocities at time $t = 0.00005$ with mesh of 500 cells; piece-wise linear IC, periodic BC. The two solutions nearly match. . . . .	30
3.3	Vertical vibrations in elastic solid: Numerical solution to the full problem with initial deformation in one dimension under the SHTC model (blue) and exact solution to the linearised problem – wave equation – (red); $y$ -positions at time $t = 0.00005$ with mesh of 500 cells; piece-wise linear IC, periodic BC. The two solutions nearly match. . . . .	31
3.4	Vertical vibrations in elastic solid: Numerical solution to the full problem with initial deformation in one dimension under the SHTC model; non-zero $x$ -velocities at time $t = 0.00005$ with mesh of 500 cells. A result not observed in the linearised problem or under the neo-Hookean model; piece-wise linear IC, periodic BC. . . . .	31
3.5	Vertical vibrations in elastic solid: Numerical solution to the full problem with initial deformation in one dimension under the SHTC model at time $t = 0.00005$ (green), $t = 0.00005 + P$ (red) and $t = 0.00005 + 2P$ (blue), where $P = \frac{1}{2141}$ is the period of the linearised elastic problem; $y$ -velocities with mesh of 500 cells; piece-wise linear IC, periodic BC. We can see a nearly periodic behaviour of the numerical solution. . . . .	32
3.6	Vertical vibrations in elastic solid: Numerical solution to the full problem with initial deformation in one dimension under the SHTC model at time $t = 0.00005$ (green), $t = 0.00005 + P$ (red) and $t = 0.00005 + 2P$ (blue), where $P = \frac{1}{2141}$ is the period of the linearised elastic problem; $y$ -positions with mesh of 500 cells; piece-wise linear IC, periodic BC. We can see a nearly periodic behaviour of the numerical solution. . . . .	32
3.7	Vertical vibrations in elastic solid: Numerical solution to the full problem with initial deformation in one dimension under the SHTC model (blue) and exact solution to the linearised problem – wave equation – (red); $y$ -positions at time $t = 0.00005$ with mesh of 500 cells; sinusoid IC, periodic BC. The two solutions nearly match. . . . .	33
3.8	Vertical vibrations in elastic solid: Numerical solution to the full problem with initial deformation in one dimension under the SHTC model at time $t = 0.00005$ (red solid line) and $t = 0.00005 + \frac{1}{2141}$ (blue dotted line); $y$ -positions with mesh of 500 cells; sinusoid IC, periodic BC. We can see a nearly periodic behaviour of the numerical solution. . . . .	33

3.9	Vertical vibrations in elastoplastic solid: Numerical solution to the problem with initial deformation in one dimension under the SHTC model with dissipation at the time $t = 0.00005$ (green), $t = 0.00005 + P$ (red) and $t = 0.00005 + 2P$ (blue), where $P = \frac{1}{2141}$ is the period of the linearised elastic problem; $y$ -velocities with mesh of 500 cells; piece-wise linear IC, periodic BC. The dissipation causes decrease in velocities. . . . .	34
3.10	Vertical vibrations in elastoplastic solid: Numerical solution to the problem with initial deformation in one dimension under the SHTC model with dissipation at the time $t = 0.00005$ (green), $t = 0.00005 + P$ (red) and $t = 0.00005 + 2P$ (blue), where $P = \frac{1}{2141}$ is the period of the linearised elastic problem; $y$ -velocities with mesh of 500 cells; sinusoid IC, periodic BC. The dissipation causes decrease in velocities. The energy lost in speed is compensated by temperature growth. . . . .	34
3.11	Vertical vibrations in elastoplastic solid: Numerical solution to the problem with initial deformation in one dimension under the SHTC model with dissipation at the time $t = 0.00005$ (green), $t = 0.00005 + P$ (red) and $t = 0.00005 + 2P$ (blue), where $P = \frac{1}{2141}$ is the period of the linearised elastic problem; temperature with mesh of 500 cells; sinusoid IC, periodic BC. . . . .	35
3.12	Simple shear in elastic solid: $y$ -velocities are plotted at five different times. Their linearity in all cases verifies that the simulated motion is close to a simple shear. . . . .	37
3.13	Simple shear in elastic solid: $x$ -velocities are plotted at five different times. Even though they are not exactly zero, they are very low. This verifies that the simulated motion is close to a simple shear. . . . .	37
3.14	Simple shear in elastic solid: Comparison of the measured relation between shear rate (measured as $A_{yx}^{-1}$ ) and computed shear stress and the analytic one found in section 3.6. . . . .	38
3.15	Simple shear in elastoplastic solid: $y$ -velocities are plotted at five different times. Their linearity in all cases verifies that the simulated motion is close to a simple shear. . . . .	38
3.16	Simple shear in elastoplastic solid: $x$ -velocities are plotted at five different times. Even though they are not exactly zero, they are very low. This verifies that the simulated motion is close to a simple shear. . . . .	39
3.17	Simple shear in elastoplastic solid: The relation between shear rate (measured as $100t$ ) and computed shear stress. Note, that it is growing sub linearly and seems to be bounded, unlike the one in elastic solid. . . . .	39
3.18	Simple shear in elastoplastic solid: The Frobenius of the Burgers tensor, which was calculated from the values of $\mathbb{A}$ by central differences. Since it is zero, integration of $\mathbb{A}$ does not depend on the integration path. . . . .	40

3.19	Simple shear in elastoplastic solid: Comparison of the real – or expected – deformation and the deformation reconstructed by integrating $\mathbb{A}^{-1}$ over the reference configuration. Even though the $\text{curl}(\mathbb{A}) = 0$ . This clearly demonstrates that the connection between reference and actual configuration is lost, considering a motion with dissipation. . . . .	40
3.20	The reference (left) and initial configuration. The blue and red lines are mapped to themselves by moving each particle only in the vertical direction; not to scale. . . . .	41
3.21	Elastoplastic solid in two dimensions; density at time $t = 0$ with $1000 \times 1000$ cells. The axes do not describe the actual position, but the cell coordinates. . . . .	42
3.22	Elastoplastic solid in two dimensions; density at time $t = 0.00001$ with $200 \times 200$ cells. One can see the expected propagation of the density from the compressed to the extended part of the body. The axes do not describe the actual position, but the cell coordinates. . . . .	42
3.23	Elastoplastic solid in two dimensions; Frobenius norm of the Burgers tensor at time $t = 0.00001$ with $200 \times 200$ cells. One can see it is non-zero around the jump in density. The axes do not describe the actual position, but the cell coordinates. . . . .	43
3.24	Couette flow between two planes at $x = 0$ and $x = 0.25$ . The velocity at $t = 0$ is zero. Five velocity profiles approximately uniformly dividing the time interval $t \in [0, 2]$ (coloured lines) are compared to the steady state linear profile (dotted line). The convergence matches the results of White [2006]. The viscosity is $\mu = 10^{-2}$ . . . . .	44
3.25	Couette flow between two planes at $x = 0$ and $x = 0.25$ . The velocity at $t = 0$ is sinusoid (blue line). Five velocity profiles approximately uniformly dividing the time interval $t \in [0, 0.5]$ (coloured lines) are compared to the steady state linear profile (dotted line). The viscosity is set to $\mu = 10^{-2}$ . The speed of convergence is significantly higher than in the case $\mu = 10^{-3}$ . . . . .	44
3.26	Couette flow between two planes at $x = 0$ and $x = 0.25$ . The velocity at $t = 0$ is sinusoid (blue line). Five velocity profiles approximately uniformly dividing the time interval $t \in [0, 2]$ (coloured lines) are compared to the steady state linear profile (dotted line). The viscosity is set to $\mu = 10^{-3}$ . The speed of convergence is significantly lower than in the case $\mu = 10^{-2}$ . . . . .	45

# List of Tables

A.1	Parameters for Ideal Gas and Shock Mie-Gruneisen equations of state used in simulations. . . . .	59
A.2	Material parameters used in simulations. . . . .	59
A.3	Dissipation parameters for materials occurring in simulations. . .	59

# A. Attachments

## A.1 Functional Derivative

Let us have  $\Omega \in \mathbb{R}^n$  open and a function  $f : \Omega \rightarrow \mathbb{R}^m$  and a functional  $F : (\mathbb{R}^m)^\Omega \rightarrow \mathbb{R}$ . Let the limit

$$\lim_{\epsilon \rightarrow 0} \frac{F(f + \epsilon \delta f) - F(f)}{\epsilon}$$

exist for every  $\delta f \in C_0^\infty(\Omega)$  and let it further be linear in  $\delta f$ .<sup>1</sup> Then we may view it as an element of the (algebraic) dual space to  $C_0^\infty(\Omega)$ . Let us denote this element by  $DF_f$ . Then we may write

$$\langle DF_f, \delta f \rangle = \lim_{\epsilon \rightarrow 0} \frac{F(f + \epsilon \delta f) - F(f)}{\epsilon}.$$

Moreover, if there exists a function  $y \in L_{Loc}^1(\Omega)$  and if we define  $T_y : T_y(\delta f) = \int y \delta f dx$  for every  $\delta f \in C_0^\infty$ , then  $T_y$  converges and is linear in  $\delta f$  and therefore belongs to  $(C_0^\infty(\Omega))^*$ . This motivates the following definition:

**Definition 1.** *Let  $f, F$  and  $\delta f$  be as above and  $g \in L_{Loc}^1(\Omega)$ . Then we say that  $g$  is the functional derivative of  $F$  with respect to  $f$  if*

$$\int_{\Omega} g \delta f dx = \lim_{\epsilon \rightarrow 0} \frac{F(f + \epsilon \delta f) - F(f)}{\epsilon}.$$

We denote the derivative by  $\frac{\delta F}{\delta f}$ .<sup>23</sup>

Furthermore, we do not need such a general approach and focus on a more specific setting, for which interesting properties hold:

Let us assume  $f$  be smooth,  $F = \int g(f(x), x) dx$ , where  $g$  is smooth and  $\int g(f + \epsilon \delta f, x)$  converge for any  $\delta f \in C_0^\infty$  and  $\epsilon$  sufficiently small. Then

$$\begin{aligned} \lim_{\epsilon \rightarrow 0} \frac{F(f + \epsilon \delta f) - F(f)}{\epsilon} &= \lim_{\epsilon \rightarrow 0} \frac{\int g(f + \epsilon \delta f, x) dx - \int g(f, x) dx}{\epsilon} \\ &= \lim_{\epsilon \rightarrow 0} \int \frac{g(f + \epsilon \delta f, x) - g(f, x)}{\epsilon} dx \\ &= \int \lim_{\epsilon \rightarrow 0} \frac{g(f + \epsilon \delta f, x) - g(f, x)}{\epsilon} dx \\ &= \int \frac{\partial g}{\partial f} \delta f dx. \end{aligned}$$

Since  $g$  is smooth, its derivative is locally integrable and thus the functional derivative has the desired form. Moreover,

$$\frac{\delta F}{\delta f} = \frac{\partial g}{\partial f}.$$

<sup>1</sup>This is guaranteed if we assume  $F$  to be Frechet differentiable. Namely, if we restrict to normed vector spaces, such as  $L^2(\Omega)$ .

<sup>2</sup>In the following text, we omit the range of integration for brevity.

<sup>3</sup>This notion is a bit confusing and it would be better from a certain point of view to denote the derivative by  $DF_f$ . We, however, use the notion common in literature.

Analogically, we may define differentiation with respect to  $f_i$ ,  $i = 1, \dots, n$  (replacing every vector  $f$  by a scalar  $f_i$ ) to get

$$\frac{\delta F}{\delta f_i} = \frac{\partial g}{\partial f_i}.$$

In the computations above, we interchanged the limit and the integral, which needs to be commented. Our aim is to use the dominated convergence theorem, i.e., we seek an integrable function dominating all integrated functions

$$\frac{g(f + \epsilon \delta f, x) - g(f, x)}{\epsilon}.$$

First, let us denote  $h_\epsilon(f, x) = g(f + \epsilon \delta f, x)$ . Since  $\delta f$  has compact support and that  $h_\epsilon(f, x) = g(f, x)$  outside that support, we realize we are in fact integrating only over the support, which is compact. Thus, the dominating function may be a constant bounding  $\frac{1}{\epsilon}(h_\epsilon(f, x) - g(f, x))$ .

Since  $\delta f$  is a  $C_0^\infty$  function, it is bounded by some constant  $C$ . From smoothness of  $g$  follows its Lipschitz continuous with some constant  $L$ . Thus  $h_\epsilon(f, x) - g(f, x)$  is bounded by  $LC\epsilon$  and  $\frac{1}{\epsilon}(h_\epsilon(f, x) - g(f, x))$  by  $LC$ . Finally we take the dominating function

$$M(x) = \begin{cases} LC, & \text{on spt}(\delta f), \\ 0, & \text{elsewhere.} \end{cases}$$

We have thus proved the following lemma.

**Lemma 1.** *Under the assumptions above,*

$$\frac{\delta F}{\delta f} = \frac{\partial g}{\partial f}.$$

## A.2 Derivation of the Governing Equations

The aim of these paragraphs is to briefly add a few details to the derivation of the governing equations in the Eulerian frame. For brevity, let us assume we want to get equation (1.1) at some  $(\mathbf{x}_1, t_1)$ . Moreover, we assume that the equations describing the time evolution are local, i.e. they depend on a neighbourhood of  $\mathbf{x}_1$  only. We assume the integrals in the Poisson bracket and the chain rule over the whole space  $\mathbb{R}^N$ . The fields  $\rho, \mathbf{m}, s, \mathbb{F}$  are assumed to be  $C^\infty$  functions over continuous body and the energy  $E$  to take the form  $\int \varepsilon(\rho, \mathbf{m}, s, \mathbb{F}) d\mathbf{x}$ , where  $\varepsilon$  is smooth. We redefine the energy into the form  $\int \varepsilon(\rho, \mathbf{m}, s, \mathbb{F}) g_1(\mathbf{x}) d\mathbf{x}$ , where  $g_1$  is a  $C_0^\infty$  function with range  $[0, 1]$  equal to 1 on some open ball  $B(x_1)$ . We redefine the fields  $\rho, \mathbf{m}, s, \mathbb{F}$  in  $\mathbb{R}^N \setminus B(x_1)$  so that they are  $C^\infty(\mathbb{R}^N)$ . Thus we change the properties of the body, but we preserve them on a neighbourhood of  $x_1$ . Further  $A$  is assumed to be in the form  $\int \rho g_2(\mathbf{x}) d\mathbf{x}$ , where  $g_2$  is a  $C_0^\infty$  function. Then, subtracting the two time evolutions of  $A$ , one gets

$$0 = \int g_2 \left[ \frac{\partial \rho}{\partial t} + \partial_i(\rho E_{m_i}) \right] d\mathbf{x}.$$

Now let us assume  $\frac{\partial \rho}{\partial t} + \partial_i(\rho E_{m_i}) \neq 0$  at  $\mathbf{x}_1$ . Then from continuity, it is WLOG positive on some open neighbourhood  $U(\mathbf{x}_1)$  of  $\mathbf{x}_1$ . Finally, taking  $g_2$  in such a way that its support lies within  $U(\mathbf{x}_1)$ , then we get the integral non-zero. Thus  $\frac{\partial \rho}{\partial t} + \partial_i(\rho E_{m_i}) = 0$  at  $\mathbf{x}_1$ , which is what we want.

### A.3 Model with Distortion Describes the neo-Hookean Solids

We would like to find the form of the stress tensor for system (1.11) – (1.14), equipped with the neo-Hookean energy. That is, we are searching the form of

$$\sigma = -\mathbb{A}^\top \varepsilon_{\mathbb{A}}$$

for the energy

$$\varepsilon = \rho \frac{\mu}{2} (\text{tr}(\mathbb{B}) - 3 - \ln(\det(\mathbb{B}))) = \rho \frac{\mu}{2} (\text{tr}(\mathbb{A}^{-1} \mathbb{A}^{-\top}) - 3 - \ln(\det(\mathbb{A}^{-1} \mathbb{A}^{-\top}))).$$

To do that, we use the chain rule. Let us now write  $\mathbb{M}' = \frac{\partial \mathbb{M}}{\partial A_{mn}}$  for any matrix  $\mathbb{M}$  depending on  $\mathbb{A}$ . Then we have  $\mathbb{I}' = (\mathbb{F}\mathbb{A})' = 0$ , which implies

$$\begin{aligned} \mathbb{F}'\mathbb{A} &= -\mathbb{F}\mathbb{A}' \\ \mathbb{F}' &= -\mathbb{F}\mathbb{A}'\mathbb{F}. \end{aligned}$$

Therefore

$$\frac{\partial F_{kl}}{\partial A_{mn}} = -F_{ka} \frac{\partial A_{ab}}{\partial A_{mn}} F_{bl} = -F_{km} F_{nl}. \quad (\text{A.1})$$

Next, realizing  $B_{ij} = F_{im} F_{jm}$ , we compute

$$\frac{\partial B_{ij}}{\partial F_{kl}} = \frac{\partial F_{im}}{\partial F_{kl}} F_{jm} + F_{im} \frac{\partial F_{jm}}{\partial F_{kl}} = \delta_{ki} \delta_{lm} F_{jm} + \delta_{jk} \delta_{lm} F_{im} = \delta_{ki} F_{jl} + \delta_{jk} F_{il}. \quad (\text{A.2})$$

Finally, we recall  $\frac{\partial \text{tr}(\mathbb{B})}{\partial B_{ij}} = \delta_{ij}$ , which altogether with (A.1) and (A.2) gives

$$\begin{aligned} \frac{\partial \text{tr}(\mathbb{B})}{\partial A_{mn}} &= \frac{\partial \text{tr}(\mathbb{B})}{\partial B_{ij}} \frac{B_{ij}}{\partial F_{kl}} \frac{F_{kl}}{\partial A_{mn}} = -\delta_{ij} (\delta_{ki} F_{jl} + \delta_{jk} F_{il}) F_{km} F_{nl} \\ &= -\delta_{ik} F_{il} F_{km} F_{nl} - \delta_{ik} F_{il} F_{km} F_{nl} = -2F_{im} F_{il} F_{nl}. \end{aligned}$$

Written in the tensor form, this is

$$\frac{\partial \text{tr}(\mathbb{B})}{\partial \mathbb{A}} = -2\mathbb{F}^\top \mathbb{B}. \quad (\text{A.3})$$

Differentiation of  $\ln(\det(\mathbb{B}))$  can be performed in a very similar way as an exercise. However, we compute it directly as

$$\frac{\partial \ln(\det(\mathbb{A}^{-1} \mathbb{A}^{-\top}))}{\partial \mathbb{A}} = \frac{\partial \ln(\det(\mathbb{A})^{-2})}{\partial \mathbb{A}} = -2 \frac{\partial \ln(\det(\mathbb{A}))}{\partial \mathbb{A}} = -2\mathbb{A}^{-\top}. \quad (\text{A.4})$$

Combining (A.3) and (A.4), we obtain

$$\sigma = \rho \mu (\mathbb{B} - \mathbb{I}),$$

which is the desired result.

## A.4 Numerical Scheme

We now describe the numerical method used to solve the equations. The ADER-WENO<sup>4</sup> numerical scheme is taken from Jackson [2017] and is described in Jackson [2017] and Jackson [2018].<sup>5</sup> To briefly summarize the most important features, it is a scheme used for solving any system of partial differential equations in the form

$$\frac{\partial \mathbf{Q}}{\partial t} + \frac{\mathbf{F}(\mathbf{Q})}{\partial \mathbf{x}} + \mathbf{B}(\mathbf{Q}) \cdot \frac{\partial \mathbf{Q}}{\partial \mathbf{x}} = \mathbf{S}(\mathbf{Q}), \quad (\text{A.5})$$

where  $\mathbf{Q} \in \mathbb{R}^N$  is the vector of state variables<sup>6</sup>,  $\mathbf{F} = (\mathbf{F}_1, \mathbf{F}_2, \mathbf{F}_3)$  is a vector of the conservative non-linear fluxes ( $\mathbf{F}_i : \mathbb{R}^N \rightarrow \mathbb{R}^N$ ),  $\mathbf{B} = (\mathbb{B}_1, \mathbb{B}_2, \mathbb{B}_3)$  ( $\mathbb{B}_i : \mathbb{R}^N \rightarrow \mathbb{R}^{N \times N}$ ) corresponds to the non-conservative terms and  $\mathbf{S} \in \mathbb{R}^N$  is the vector of source terms. Note that (A.5) can be reformulated to

$$\frac{\partial \mathbf{Q}}{\partial t} + \mathbf{M}(\mathbf{Q}) \cdot \frac{\partial \mathbf{Q}}{\partial \mathbf{x}} = \mathbf{S}(\mathbf{Q}),$$

where  $\mathbf{M} = (\mathbb{M}_1, \mathbb{M}_2, \mathbb{M}_3)$ ,  $\mathbb{M}_i = \frac{\partial \mathbf{F}_i}{\partial \mathbf{Q}} + \mathbb{B}_i$ .

The method first uses the WENO method to approximate the given cell-wise constant  $\mathbf{Q}$  by a polynomial of any given order. Then a spatio-temporal polynomial of the same order is reconstructed by the discontinuous Galerkin method and finally, finite volumes with Rusanov fluxes are implemented. In the next paragraphs we briefly summarize the key ideas of the numerical scheme. For more details, the reader may see Jackson [2018] or other sources mentioned above. We also restrict ourselves to the one-dimensional case.

### WENO Method

Let us consider the domain  $[0, L]$  and natural numbers  $K, N$ .  $N$  describes the degree of polynomials used, causing the method to be of order  $N + 1$ , while  $K$  is the number of cells in which we divide the domain. The grid points are denoted by  $x_i = \frac{iL}{K}$  and their difference by  $\Delta x = \frac{L}{K}$ . Let us denote the cell  $[x_i, x_{i+1}]$  by  $C_i$ . We assume we have cell-wise constant  $u$  on  $[0, L]$  and approximate the data on  $C_i$  by a polynomial of an order  $N$ . Let us define

$$\chi^i(x) = \frac{1}{\Delta}(x - x_i)$$

and denote the Gauss-Legendre abscissae on  $[0, 1]$  by  $\{\chi_0, \dots, \chi_N\}$ . Now let us define the Lagrange interpolating polynomials  $\psi_i$  of order  $N$  as fulfilling

$$\psi_i(\chi_j) = \delta_{ij}.$$

The data on  $C_i$  is then reconstructed by

$$w_i(x) = \sum_p \psi_p(\chi_i(x)) w_p^i,$$

where the weights  $w_p^i$  are described by Jackson [2018].

<sup>4</sup>Stands for ‘‘Advection-Diffusion-Reaction’’ and ‘‘Weighted Essentially Non-Oscillatory’’.

<sup>5</sup>For further reading about closely related numerical methods, the reader is kindly advised to see Tiarev and Toro [2001], Boscheri et al. [2016], or Dumbser et al. [2018].

<sup>6</sup>in our case  $\rho, \varepsilon, \mathbf{m}$  and  $\mathbb{A}$ .

## Discontinuous Galerkin Method

Let us now assume we have performed the WENO reconstruction at time  $t_n$ . We want to approximate the solution  $Q$  on  $C_i \times [t_n, t_{n+1}]$ . Let us denote  $\Delta t_n = t_{n+1} - t_n$  and re-scale the time variable to

$$\tau^n(t) = \frac{1}{\Delta t_n}(t - t_n).$$

Then (A.5) becomes:

$$\frac{\partial \mathbf{Q}}{\partial \tau^n} + \frac{\mathbf{F}^*(\mathbf{Q})}{\partial \chi^i} + \mathbf{B}^*(\mathbf{Q}) \cdot \frac{\partial \mathbf{Q}}{\partial \chi^i} = \mathbf{S}^*(\mathbf{Q}), \quad (\text{A.6})$$

where

$$\mathbf{F}^* = \frac{\Delta t_n}{\Delta x} \mathbf{F}, \quad \mathbf{B}^* = \frac{\Delta t_n}{\Delta x} \mathbf{B}, \quad \mathbf{S}^* = \Delta t_n \mathbf{S}.$$

Now we define the basis functions in space and time as

$$\{\theta_k(\chi, \tau)\} = \{\psi_p(\chi), \psi_s(\tau), 0 \leq p, s \leq N\}$$

and approximate

$$\begin{aligned} \mathbf{Q} &\approx \theta_k \mathbf{Q}_k, \\ \mathbf{F}^*(\mathbf{Q}) &\approx \theta_k \mathbf{F}_k, \\ \mathbf{B}^*(\mathbf{Q}) \cdot \frac{\partial \mathbf{Q}}{\partial \chi} &\approx \theta_k \mathbf{B}_k, \\ \mathbf{S}^*(\mathbf{Q}) &\approx \theta_k \mathbf{S}_k. \end{aligned}$$

Thus, one has

$$\begin{aligned} \mathbf{F}_k &= \mathbf{F}^*(\mathbf{Q}_k), \\ \mathbf{B}_k &= \mathbf{B}^*(\mathbf{Q}_k) \cdot \left( \frac{\partial \theta_m(\chi_k, \tau_k)}{\partial \chi} \mathbf{Q}_m \right), \\ \mathbf{S}_k &= \mathbf{S}^*(\mathbf{Q}_k), \end{aligned}$$

where  $(\chi_k, \tau_k)$  is the node corresponding to  $\theta_k$ .

Multiplying (A.6) by  $\theta_l$ , using the approximations, integrating over space-time cell in scaled variables and employing the integration by parts in time, one gets

$$\begin{aligned} &\left( \int \theta_l(\chi, 1) \theta_k(\chi, 1) d\chi - \int \frac{\partial \theta_l}{\partial \tau}(\chi, \tau) \theta_k(\chi, \tau) d\chi d\tau \right) \mathbf{Q}_k = \\ &= \int \theta_l(\chi, 0) w_i(\chi) d\chi - \int \frac{\partial \theta_k}{\partial \tau}(\chi, \tau) \theta_l(\chi, \tau) d\chi d\tau \mathbf{F}_k \\ &\quad + \int \theta_l(\chi, \tau) \theta_k(\chi, \tau) d\chi d\tau (\mathbf{S}_k - \mathbf{B}_k), \end{aligned}$$

where  $w_i$  is the approximation by the WENO method. This is a non-linear system in  $\mathbf{Q}_k$  and it is solved by a Newton method. The resulting approximation is denoted by  $\mathbf{Q}_{\text{approx}}$ .

## Finite Volumes

Integration of (A.5) over  $C_i \times [t_n, t_{n+1}]$  yields

$$\mathbf{Q}_i^{n+1} = \mathbf{Q}_i^n + (\mathbf{S}_i^n - \mathbf{P}_i^n) - (\mathbf{D}_{i+1}^n - \mathbf{D}_i^n),$$

where

$$\begin{aligned} \mathbf{Q}_i^n &= \int_{x_i}^{x_{i+1}} \mathbf{Q}(x, t_n) dx, \\ \mathbf{S}_i^n &= \int_{t_n}^{t_{n+1}} \int_{x_i}^{x_{i+1}} \mathbf{S}(\mathbf{Q}) dx dt, \\ \mathbf{P}_i^n &= \int_{t_n}^{t_{n+1}} \int_{x_i}^{x_{i+1}} \mathbf{B}(\mathbf{Q}) \cdot \frac{\partial \mathbf{Q}}{\partial x} dx dt, \\ \mathbf{D}_i^n &= \int_{t_n}^{t_{n+1}} D(\mathbf{Q}^-(x_i, t), \mathbf{Q}^+(x_i, t)) dt. \end{aligned}$$

Here,  $\mathbf{Q}^-(x_i, t)$  and  $\mathbf{Q}^+(x_i, t)$  are the left and right limits of  $\mathbf{Q}$  to  $x_i$ .  $\mathbf{S}_i^n$ ,  $\mathbf{P}_i^n$  and  $\mathbf{D}_i^n$  computed by an  $N+1$ -point Gauss-Legendre quadrature, where  $\mathbf{Q}$  is replaced by  $\mathbf{Q}_{\text{approx}}$ .

The last thing needed is to specify the numerical flux  $D$ . First, let us recall  $\mathbf{M} = \frac{\partial \mathbf{F}}{\partial \mathbf{Q}} + \mathbf{B}$  and  $\Lambda$  its eigenvalues. The flux is then defined as

$$D(\mathbf{Q}^-, \mathbf{Q}^+) = \frac{1}{2} \left( \mathbf{F}(\mathbf{Q}^-) + \mathbf{F}(\mathbf{Q}^+) + \hat{\mathbf{B}} \cdot (\mathbf{Q}^+ - \mathbf{Q}^-) - \hat{\mathbf{M}} \cdot (\mathbf{Q}^+ - \mathbf{Q}^-) \right),$$

where

$$\hat{\mathbf{B}} = \int_0^1 \mathbf{B}(\mathbf{Q}^- + z(\mathbf{Q}^+ - \mathbf{Q}^-)) dz$$

and  $\hat{\mathbf{M}}$  represents the Rusanov flux

$$\hat{\mathbf{M}} = \max \left( \max |\Lambda(\mathbf{Q}^-)|, \max |\Lambda(\mathbf{Q}^+)| \right).$$

## Boundary Conditions

The boundary conditions are implemented by ghost cells. Let us call  $C_l^{\text{in}}$  and  $C_r^{\text{in}}$  the left and right edge cells and  $C_l^{\text{out}}$  and  $C_r^{\text{out}}$  the respective ghost cells. For periodic boundary conditions, the state variables in  $C_l^{\text{out}}$  are set equal to  $C_r^{\text{in}}$  and similarly on the other side. For no-slip, the state variables in  $C_l^{\text{out}}$  are copied from  $C_l^{\text{in}}$  with the exceptions that the speed is altered to  $v_l^{\text{out}} = -v_l^{\text{in}} + 2v_l$ , where  $v_l$  is the prescribed speed of the left boundary. The energy is then recalculated to capture the change of kinetic energy. Analogous procedure is implemented on the right hand side.

## A.5 Material Properties

Material parameters used in numerical simulations throughout this text are presented in the tables below. All values are given in SI units.

Material Modelled	EOS <sup>a</sup> used	$\gamma$	$\Gamma_0$	$\mathbf{u}$	$\mathbf{c}_0$	$\mathbf{T}^{\text{ref}}$
Fluid	Ideal Gas	1.4	—	—	—	0
Solid	Shock Mie-Gruneisen	—	2	1.5	3939	300

*Note:* <sup>a</sup> Equation of state.

Table A.1: Parameters for Ideal Gas and Shock Mie-Gruneisen equations of state used in simulations.

Material Modelled	$\rho_0$	$\mathbf{p}_0$	$\mathbf{c}_v$	$\mathbf{c}_s$
Fluid	1	1/1.4	1	1
Solid	8930	0	390	2141

Table A.2: Material parameters used in simulations.

Material Modelled	$\mu^a$	$\tau_0$	$\sigma_0$	$\mathbf{n}$
Fluid	$10^{-2}/10^{-3}$	—	—	—
Solid	—	1	$9 \times 10^7$	50

*Note:* <sup>a</sup> Dynamic viscosity.

Table A.3: Dissipation parameters for materials occurring in simulations.